Journal of
Materials Chemistry A

Materials for energy and sustainability

rsc.li/materials-a

ROYAL SOCIETY
OF **CHEMISTRY**

REVIEW ARTICLE
Febri Baskoro, Hung-Ju Yen *et al.*
Recent advances in p-type polymeric electrode materials
towards high-voltage 4.0 V-class organic lithium-ion
batteries

REVIEW

Check for updates

Recent advances in p-type polymeric electrode materials towards high-voltage 4.0 V-class organic lithium-ion batteries

Febri Baskoro, ORCID †*ab Santosh U. Sharma,†a Andre Lammiduk Lubis ORCID a and Hung-Ju Yen ORCID *ac

Lithium-ion batteries stand at the forefront of energy storage technologies, facilitating the transition towards sustainable and electrified systems. However, to meet the increasing demands for energy density, safety, and longevity, the development of high-performance electrode materials is paramount. Although inorganic materials have been dominant in the current lithium-ion battery cathodes, the widely utilized inorganic cathode materials suffer from drawbacks, such as limited capacity, high energy consumption during their production, safety hazards associated with toxic metals (Li, Co, Mn, and Ni), and high raw material costs, due to their limited or localized resource distributions. Alternatively, polymeric materials have emerged as promising candidates to replace conventional inorganic materials due to their advantages such as abundance, environmentally friendly resources, structural diversity, ease of functionalization, fabrication, recycling, high capacity and rate capability, and excellent flexibility. This review article explores the strategic design principles underlying the synthesis and optimization of p-type polymeric electrode materials for next-generation 4.0 V-class batteries. Through a comprehensive analysis of recent advancements, morphology control, and interface engineering, this review elucidates

aInstitute of Chemistry, Academia Sinica, Taipei 115, Taiwan. E-mail: febri_baskoro@yahoo.co.id; hjyen@gate.sinica.edu.tw

bMaterial Science and Engineering Research Group, Faculty of Mechanical and Aerospace Engineering, Institut Teknologi Bandung, Jl. Ganesha 10, Bandung 40132, Indonesia

cSustainable Chemical Science and Technology Program, Taiwan International Graduate Program (TIGP), Academia Sinica and National Taiwan University, Taipei 11529, Taiwan

† These authors contributed equally.

Febri Baskoro

Dr Febri Baskoro obtained his PhD in Sustainable Chemical Science and Technology from National Yang Ming Chiao Tung University, Taiwan, in 2021, a joint PhD program between the Institute of Chemistry, Academia Sinica, and National Yang Ming Chiao Tung University, Taiwan. He earned his BS from Sebelas Maret University, Indonesia, and MS from Chang Gung University, Taiwan. Currently, he works as an Academia Sinica Postdoctoral Research Fellow in the Institute of Chemistry, Academia Sinica, Taiwan, under the guidance of Dr Hung-Ju Yen. His research interests include the development of novel functional electrode materials including MOFs, nanographenes, organic molecules, and polymers for high-performance and sustainable batteries.

Santosh U. Sharma

Dr Santosh U. Sharma completed his PhD in polymeric material chemistry for energy storage applications, such as lithium-ion batteries and super-capacitors, under the guidance of Prof. Jyh-Tsung Lee at National Sun Yat-sen University, Taiwan. He holds an MS in Industrial Polymer Chemistry and a BS in Chemistry, both from the University of Mumbai, India. Currently, he is a Post-doctoral Researcher at the Institute of Chemistry, Academia Sinica, Taiwan, working in Dr Hung-Ju Yen's group. His research interest includes the development and synthesis of redox-active molecules, including small molecules, polymers, and porous materials, for batteries and supercapacitors.

1552 | *J. Mater. Chem. A*, 2025, **13**, 1552–1589

This journal is © The Royal Society of Chemistry 2025

the key strategies employed to achieve high-energy-density electrodes. Additionally, this review discusses the fundamental mechanisms governing the electrochemical performances of p-type polymeric electrodes and highlights the emerging trends and future directions in this field. By integrating insights from materials science, electrochemistry, and engineering, this review provides a roadmap for the rational design and development of p-type polymeric electrode materials towards the realization of high-performance 4.0 V-class lithium-ion batteries.

1. Introduction

In today's fast-paced and interconnected world, lithium-ion batteries (LIBs) have emerged as the linchpin of modern society, powering a vast array of devices that have become essential to our daily lives. From smartphones and laptops to electric vehicles (EVs) and renewable energy storage grids, LIBs serve as the backbone of our digital economy and the catalyst for the transition towards a sustainable energy future.[1–3] As the world's dependency on LIBs continues to deepen, driven by advancements in technology, evolving consumer preferences, and global efforts to combat climate change, it becomes increasingly imperative to understand their significance, challenges, and prospects. However, the reliance on LIBs also presents challenges, including the need for improved safety, environmental impact of raw material extraction, and development of effective recycling strategies to manage end-of-life batteries.[4] These challenges must be addressed to ensure the sustainable growth of LIB technology. In this regards, innovations in battery chemistry, design, and manufacturing processes are expected to further improve the energy density, safety, and lifecycle of LIBs, contributing to their continued importance in a low-carbon future.[5]

Generally, a conventional LIB cell consists of a positive electrode (cathode), negative electrode (anode), and non-aqueous electrolyte system as well as a separator to prevent physical contact between these two electrodes (Fig. 1a). In principle, when a battery is being charged, the Li^+ ions move from the cathode to anode through the electrolyte, whereas during discharge, the Li^+ ions will move back from the anode to the cathode, releasing electrical current. As cathode materials, typical Li-intercalated materials, such as $LiCoO_2$ (a lithium metal oxide with layered structure), have been widely used as lithium-ion sources. Meanwhile, graphite has been widely utilized as the anode material to store Li^+ in its layers *via* the intercalation process. Notably, both the cathode and anode materials should be able to reversibly insert and remove Li^+ from their respective structures.[7] Furthermore, given that the cell voltage is established by the energy difference between the anode and cathode, the cathode energy should lie as low as possible, and the anode must lie as high as possible. This implies that cathode materials would require the stabilization of their higher oxidative states with a lower-lying energy band, while the anode materials would require the stabilization of their lower oxidative states with a higher-lying energy band.[6,8,9] The electrolyte is the third component of LIBs, which serves as a medium to transport the Li^+ ions involved in charging/discharging process of the LIBs.[10] Although the role of the electrolytes is often considered trivial, the choice of electrolyte system is crucial depending on its compatibility with both electrodes.[11] Besides the importance and technological advancement in the LIB components, the development of cathode materials has attracted research interest given that they play an important role in defining the working potential of LIB cells, thus having a significant impact on the energy density of the battery.

1.1 Current-status of cathode materials for LIBs

Given that the cathode materials are key in determining the cell voltage and, consequently, its energy density, the high-energy-

Andre Lammiduk Lubis obtained his Master's Degree in Chemistry from National Chung Hsing University, Taiwan, in 2021 under the supervision Prof. Kuan-Jiuh Lin. He was a Research Assistant in Dr Hung-Ju Yen's group in the Institute of Chemistry, Academia Sinica, Taiwan, in 2021–2024. His works mainly focus on the testing of polymer-based electrode materials for lithium-ion batteries.

Andre Lammiduk Lubis

Dr Hung-Ju Yen is an Assistant Research Fellow in the Institute of Chemistry at Academia Sinica. He earned his BS (2006) and MS (2007) from National Chi Nan University and then completed his PhD with the 1st prize among all PhD graduates from National Taiwan University (NTU) in 2011. He joined Los Alamos National Laboratory as a J. Robert Oppenheimer Fellow (2013–2017) after his postdoctoral training at NTU

Hung-Ju Yen

(2011, 2012–2013). Dr Yen's main research interest lies in the organic synthesis of functional nanographenes and electroactive polymers for optoelectronic and energy applications.
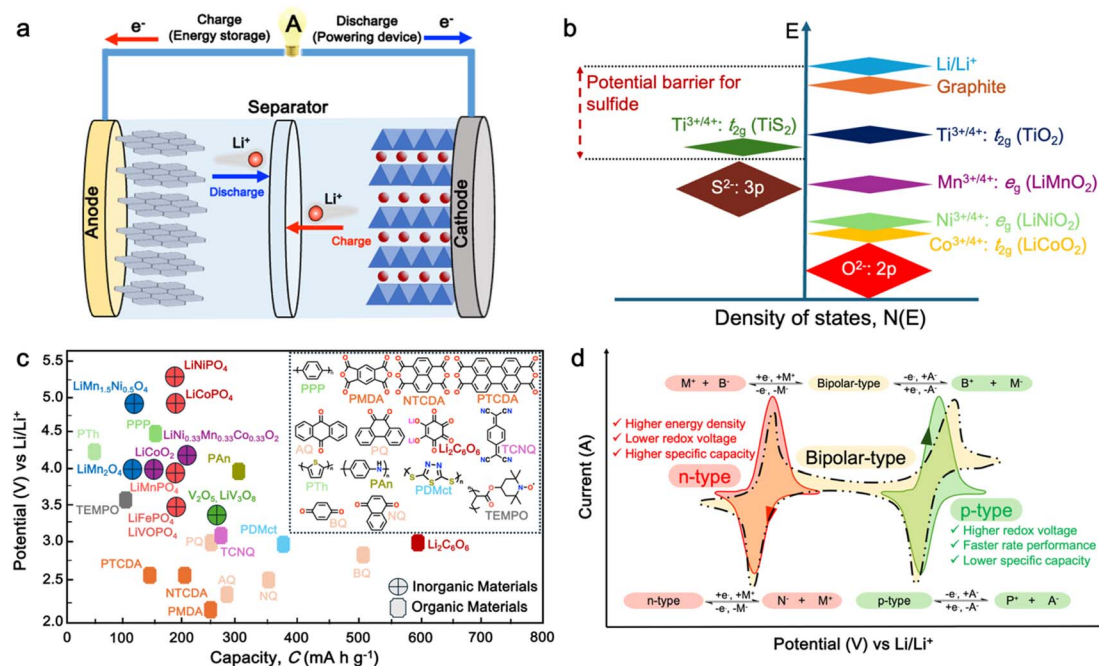
This journal is © The Royal Society of Chemistry 2025

J. Mater. Chem. A, 2025, **13**, 1552–1589 | **1553**

Fig. 1 (a) Schematic of a full cell Li–ion battery. (b) Positions of the redox energies relative to the top of the anion: p bands. The top of the S^{2-}: 3p band lying at a higher energy limits the cell voltage to <2.5 V with a sulfide cathode. In contrast, the top of the O^{2-}: 2p band lying at a lower energy enables access to lower–lying energy bands with higher oxidation states and increases the cell voltage substantially to ~4 V. Reproduced from ref. 6. (c) Recent development of cathode materials for LIBs. (d) Redox behavior of organic molecules in electrochemical processes.

density batteries require high working potential cathodes, paired with anodes that can provide a high specific capacity.[2] In early study of LIB cathodes, Goodenough employed the basic understanding that the top of the S^{2-}: 3p band lies at a higher energy than the top of the O^{2-}: 2p band to design oxide cathodes (Fig. 1b). This means that the access to lower-lying energy bands with higher oxidation states such as $Co^{3+/4+}$, and hence a higher cell voltage will be limited by the top of the S^{2-}: 3p band, and attempts to lower the cathode redox energy by accessing higher oxidation states in a sulfide will result in the oxidation of the S^{2-} ions to molecular disulfide ions $(S_2)^{2-}$. In contrast, in an oxide, the cathode redox energy can be significantly lowered by accessing lower-lying energy bands such as $Co^{3+/4+}$, and hence the cell voltage can be increased to as high as 4 V given that the top of the O^{2-}: 2p band lies at a lower energy compared to the top of the S^{2-}: 3p band. This basic idea led to the discovery of oxide cathodes materials such as layered oxide, spinel oxide, and polyanion cathodes.[6,8,9]

In general, the most common cathode materials used in commercial LIBs are based on transition metal oxides (Fig. 1c), such as lithium cobalt oxide $(LiCoO_2)$,[12] lithium manganese oxide $(LiMn_2O_4)$,[13] lithium nickel manganese cobalt oxide $(LiNiMnCoO_2$ or NMC),[14] and lithium iron phosphate $(LiFePO_4$ or LFP).[15,16] However, they suffer from gradual capacity fading during cycling, which is attributed to the dissolution of the transition metal ions in the electrolyte, leading to their accumulation on the electrode, and thus resulting in a high resistive solid electrolyte interphase (SEI) layer on the cathode surface.[17,18] Furthermore, there are several persisting challenges associated with the development of inorganic-based cathode

materials.[19–22] Firstly, with the increasing demand for high energy density batteries, there is a limitation in the theoretical capacity and working potential of current inorganic-cathode materials.[23] Secondly, the high cost of raw materials due to their scarcity and environmental burden.[6] Furthermore, complex and high-temperature synthesis processes are required, thus further increasing the material cost.[24] Thirdly, the safety issue associated with unstable cathode materials such as $LiCoO_2$, which can pose thermal runaway risks at high voltages, potentially leading to fires or explosions.[25]

Alternatively, organic cathode materials have emerged as promising contenders in the pursuit of next-generation energy storage solutions (Fig. 1c). Organic materials composed of elements such as C, O, N, and S have been recognized as a promising alternative to inorganic materials for battery electrodes.[26] These materials have several advantages, including abundance, light weight, and environmental benignity.[3,27,28] They can be used in various types of batteries, including metal-ion,[29] dual-ion,[30,31] molecular-ion,[32] and anion-shuttle batteries,[33] without being limited by the choice of counterions. Additionally, the flexible intermolecular packing of these materials has the potential to provide a higher rate capability than that of inorganic materials.[3,27] Most importantly, the physicochemical and electrochemical properties of these materials can be easily tailored through elaborate molecular design.[34]

In general, electroactive organic materials can be broadly classified into three categories based on their charge states during redox reactions, namely p-type, n-type, and bipolar-type (Fig. 1d). As shown in Fig. 1d, p-type materials undergo

1554 | J. Mater. Chem. A, 2025, 13, 1552–1589

This journal is © The Royal Society of Chemistry 2025

oxidation from their neutral state, resulting in a positively charged state, while n-type materials accept an electron and become negatively charged.[35] Bipolar-type materials usually contain both p- and n-type moieties, which can utilize both positively and negatively charged states. The specific moiety or redox center in the organic molecule governs the electrochemical response and defines the material type. Comparing the organic-based cathodes, p-type organic electrodes generally have higher redox potentials than that of n-type materials due to their lower electron energy level, thus resulting in higher redox potentials.[36] Notably, the type of redox material should be carefully considered in understanding its electrochemical mechanism, given that it is sensitive to the nature of the anion and cation dissolved in the electrolyte. For example, the electrochemical activity of p-type materials is affected by the type of anions in the electrolyte. The anions in the electrolyte can coordinate with the redox centers of p-type materials, influencing their electrochemical behavior.[36] Meanwhile, in n-type materials, the positively charged cations (Li^+, K^+, Na^+, *etc.*) determine their electrochemical behavior such as voltage, specific capacity and cyclability.[29,37–39]

However, although organic materials offer many benefits as alternative electrode materials in LIBs, they still face some challenges that need to be addressed.[27] One major hurdle is their typically low electronic conductivity, which can limit the rate capability and overall performance of the battery.[40,41] Stability and cyclability are also critical considerations for organic cathode materials. Some organic compounds may suffer from poor stability over repeated charge–discharge cycles, leading to capacity fading and a reduced battery life.[42] Additionally, solubility in the electrolyte poses a challenge for certain organic cathode materials. The dissolution of the active molecules in the electrolyte can result in capacity loss and electrolyte degradation over time.[43,44] In brief, both inorganic and organic materials play distinct roles as cathode materials for LIBs. Although inorganic cathodes are currently dominant in commercial applications, ongoing research into organic cathodes promises advancements that can lead to more sustainable and cost-effective energy storage solutions.

1.2 Definition of polymeric electrodes

To improve the stability and cyclability of organic-based electrode materials, several approaches have been explored such as polymerization,[45–47] use of high-concentration electrolytes,[48,49] nanostructures,[50–53] and composite formation with advanced carbon materials.[54–57] Among them, the polymerization process is considered a significant strategy that can solve the dissolution problem and improve the material stability of organic-based electrodes in the electrolyte.[58–63] Since then, the definition of polymeric electrodes in LIBs have emerged as a type of electrode material made from polymer-based materials. Polymer-based materials are known for their flexibility, conductivity, and chemical stability, making them suitable for use in various electrochemical devices such as batteries and capacitors.[28] Furthermore, their design can be easily customized at the molecular level to meet specific energy storage requirements.

Benefiting from organic-based cathodes and their excellent physical properties, polymeric electrodes have emerged as of new class of electrode materials to replace traditional inorganic electrodes in LIBs. Furthermore, polymeric materials have been proven to be the active component, which can serve as either the anode, cathode or both electrodes in an LIB setup.[58,62–65] Unlike small-organic molecules, which have a major concern in terms of their inherent solubility in organic electrolytes and thus limits their widespread use and development, the higher molecular weight of polymer electrode materials often reduces their solubility in organic electrolytes, making them more promising candidates for the next generation of LIBs.[66] One of unique properties of polymer-based electrodes is their flexibility, given that polymeric electrodes can be made into flexible films, thus opening a way for the fabrication of flexible batteries. Additionally, polymeric materials are generally less expensive than inorganic materials, making them a cost-effective alternative.[67] Furthermore, polymeric materials are more environmentally friendly than inorganic materials, given that they do not require the mining and processing of heavy metals. This distinction underscores the potential of these polymers as a favorable trend in advancing LIB technologies. However, despite these advantages, polymeric electrodes also face some limitations, which need to be addressed. One major limitation is their lower electrical conductivity compared to inorganic materials. This can result in a lower charge transfer efficiency and reduced battery performance.[27] Additionally, polymeric materials generally have lower lithium-ion conductivity than inorganic materials, which can lead to slower ion transport and reduced battery performance.[3]

Earlier studies have shown that conducting polymers (CPs) such as polythiophene (PTh), polypyrrole (PPy), and polyaniline (PANI) can be oxidized by accepting anions, which significantly increases their electrical conductivity, and thus applied in rechargeable batteries.[68–71] However, their use is limited due to their low specific capacity and sloppy voltage profiles. Furthermore, nitroxide radical polymers, which can undergo bipolar-type redox reactions, have also been proposed as alternative organic cathode materials.[72] These polymers can accept an anion or cation, which allows them to undergo single-electron oxidation (p-type) or single-electron reduction (n-type). However, their low electrical conductivity and high solubility made them impractical.[73,74] Since then, many researchers have focused on n-type organic electrode materials[75–78] such as benzoquinone,[79] anthraquinone,[80] terephthalate,[81] and imide[53,82] derivatives. However, the redox voltage of these n-type organic materials is typically limited to below 3.0 V *vs.* Li/Li$^+$, which is inferior to that of conventional cathode materials due to their redox mechanism (Fig. 1c).

Alternatively, high redox voltage p-type organic materials such as phenazine,[83,84] carbazole,[85,86] and phenylamine[87,88] derivatives are gaining attention for their application in LIBs. These materials undergo reversible oxidations to form cationic species, which can lead to a faster rate performance. For example, phenoxazine (**PXZ**)-based cathodes exhibited a specific capacity of 112 mA h g^{-1} at 1C with an average discharge voltage of 3.7 V *vs.* Li/Li$^+$ and retained 73% capacity at a high rate of 20C.[89] A benzo[*b*]phenazine-based polymer (***p*-DPBPZ**) displayed

This journal is © The Royal Society of Chemistry 2025

J. Mater. Chem. A, 2025, **13**, 1552–1589 | **1555**

an initial discharge specific capacity of 151 mA h g^{-1}, with energy and power densities reaching 537 W h kg^{-1} and 1965 W kg^{-1}, respectively.[90] Furthermore, indole[3,2-b]carbazole (**DEICZ**) showed stable plateaus at high discharge potentials of 3.44 V and 4.09 V vs. Li/Li$^+$.[91] Moreover, materials based on the extended π–π conjugation of dioxin have also been reported to surpass the redox potential limit of organic cathode materials, achieving high voltages of over 4.1 V.[92] Additionally, based on the structural design of polymer electrodes, we successfully combined the triphenylamine (p-type) and naphthalimide (n-type) moieties in a polymer backbone, resulting in a significant increase in specific capacity and working voltage up to ~202 mA h g^{-1} and 4.5 V vs. Li/Li$^+$, respectively.[62] Furthermore, our studies also found that conformational structures (isomerism) and bridge functionalization on the imide units impact the electrochemical performance of polymer electrodes by regulating their intrinsic properties such as charge storage behavior, ion diffusivity, and activation energy.[62–64] These examples underscore the potential of polymer electrode materials and the importance of structural design in the polymer structure to achieve a high energy density and fast charge–discharge rates as well as high-voltage ability, making them promising candidates for advanced LIBs. Herein, we delve into the cutting-edge advancements in designing high-voltage p-type organic cathode materials for LIBs. We explore a variety of p-type organic materials that have emerged over the last decade, each based on distinct redox-active centers. Our discussion encompasses their electrochemical attributes, such as redox potentials and kinetics, and how these properties influence the overall performance of LIBs. By providing a comprehensive overview of the progress in p-type organic materials, we aim to highlight their potential to revolutionize the design of high-voltage polymer-based cathodes for LIB applications through a comparison of the molecular design strategies employed.

2. Requirement, properties, and challenges of polymer electrodes

2.1 General requirements of LIB cathode materials

The cathode plays a pivotal role in LIBs given that it serves as both the source and recipient of lithium ions during the charge and discharge cycles, and also define the working potential of LIB cells. To ensure the optimum performance, several aspects need to be considered in the design of next-generation cathode materials as, follows:[93–95]

(i) Redox-active ion: the presence of a redox-active ion is crucial given that it enables the material to undergo reversible oxidation and reduction processes during the charge and discharge cycles. This redox activity allows the storage and release of lithium ions, contributing to the overall capacity of the battery. In general, materials with well-defined redox chemistry can exhibit high energy density and excellent cycling stability, making them ideal candidates for high-performance battery electrodes.

(ii) Reversible lithium reaction: the ability of the material to undergo reversible reactions with lithium ions is essential for maintaining the integrity of the host structure throughout multiple charge and discharge cycles. This reversible process ensures that the active material can efficiently accommodate and release lithium ions without significant structural degradation. Furthermore, a stable host structure not only prolongs the cycle life of the battery but also helps maintain its energy storage capacity over time.

(iii) High free energy of reaction: a high free energy reaction with lithium ions is desirable given that it directly correlates with the capacity of the battery electrode material. Materials with a high capacity can store a greater number of lithium ions per unit mass, leading to enhanced energy storage capabilities. Achieving a voltage of around 4 V, while considering the stability of the electrolyte is crucial for maximizing the energy density of LIBs and meeting the demands of high-energy storage applications.

(iv) Ionic electrical conductivity: high-power density in LIBs relies on the rapid kinetics of lithium-ion insertion/extraction and fast electronic conductivity within the electrode material. Fast lithium diffusion rates and low activation energies enable swift ion transport, ensuring efficient electrochemical reactions. This facilitates rapid energy transfer, which is ideal for applications such as electric vehicles and portable electronics. Additionally, high electrical conductivity can minimize the resistance and voltage losses during the electrochemical process, thus further enhancing the overall energy density and efficiency.

(v) Structural stability: maintaining structural stability is crucial to prevent mechanical deformation, pulverization, or structural collapse of the electrode material during prolonged cycling. Structural stability ensures that the active material retains its integrity and functionality, contributing to the long-term performance and cycle life of the battery. Materials with robust structures exhibit excellent mechanical strength and resistance to degradation, even under extreme operating conditions, enhancing the reliability and safety of LIB systems.

(vi) Cost-effectiveness and environmental challenges: cost-effectiveness and environmental considerations play pivotal roles in the development of LIB materials. Economically feasible materials not only enable widespread adoption by reducing manufacturing costs but also contribute to the competitiveness of LIBs in various markets, fostering innovation and advancement in battery technology. Addressing environmental concerns by utilizing non-toxic, recyclable, and sustainably sourced materials helps minimize the ecological footprint of batteries, aligning with global efforts towards a cleaner and more sustainable future. Furthermore, promoting the use of environmentally benign materials encourages the development of greener battery technologies, supporting the transition to renewable energy systems and reducing dependence on finite resources.

2.2 Properties of p-type polymer electrode

The redox potential of a material is a critical factor in determining its suitability for use in energy storage devices. The redox potential is influenced by the molecular structure of the

1556 | J. Mater. Chem. A, 2025, **13**, 1552–1589
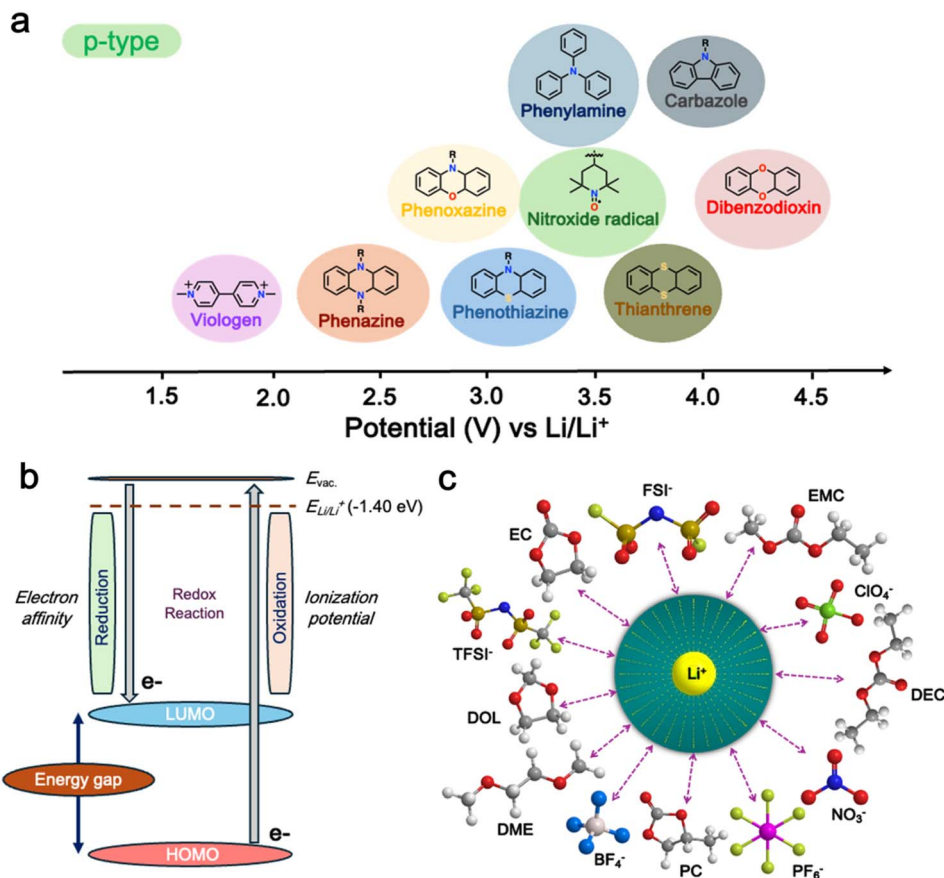
This journal is © The Royal Society of Chemistry 2025

Fig. 2 (a) Different p-type organic materials along with their average redox voltages. (b) Frontier molecular orbitals (FMOs) relevant to the redox reactions of redox-active organic materials. (c) Schematic showing a solvated anion and cation within the electrolyte. Reproduced from ref. 36.

material and the nature of the electrolyte used.[96] In the case of p-type materials, their redox potential is higher than that of n-type materials, making them more suitable for use as cathodes in energy storage devices (Fig. 2a). At the core of their functionality, their conjugated molecular structure, featuring alternating single and double bonds along the polymer backbone, enables the delocalization of electrons, and thus facilitates the movement of charge carriers through the material.[97,98] Furthermore, p-type polymers offer tunable energy levels through chemical modifications, which allows precise engineering of their electronic properties to match specific device requirements.[99,100] Moreover, p-type polymers have also been recognized to provide good thermal and structural stability, which is essential for withstanding the processing and operational conditions of electronic devices.[101] Some p-type polymers can be designed to be air-stable, thus eliminating the need for stringent inert atmospheres during the device fabrication.[102,103] Additionally, their high charge carrier mobility, compatibility with other materials used in device architectures, and relatively low bandgap further contribute to their versatility and suitability for a wide range of applications.[104–106]

Furthermore, in p-type organic cathode materials, their performance is significantly affected by factors such as redox voltage and energy levels, as well as the impact of counter ions.[36,89] The redox potential of p-type organic cathode materials

is crucial for their electrochemical performance, which is determined by their highest occupied molecular orbital (HOMO) energy level (Fig. 2b).[36] Therefore, adjusting this HOMO level of p-type organic cathode materials through heteroatom doping and functionalization can further optimize their performance in energy storage applications.[107] Meanwhile, the counter ions, such as BF_4^-, PF_6^-, FSI^-, and $TFSI^-$, also significantly impact the performance of p-type organic cathode materials including their charge transport properties, ionic conductivity, and ultimately their storage capacity and power density (Fig. 2c).[108] Overall, p-type polymers offer a combination of properties that make them promising candidates for cathode materials in LIBs.[36,109]

2.3 Challenges and limitations

P-type polymers possess unique properties, which make them attractive for various applications, including energy storage such as LIBs. These polymers are characterized by their ability to accept and transport charge ions within their structure. This property stems from the presence of electron-deficient units or dopants within the polymer backbone. Apart from the outstanding properties that have been elaborated in the previous section, the development of p-type polymer electrodes faces certain challenges, as follows:[36,66,110–116]

This journal is © The Royal Society of Chemistry 2025

J. Mater. Chem. A, 2025, 13, 1552–1589 | 1557

(i) Susceptibility to degradation: given that p-type polymer cathodes offer a high voltage operation, and thus maintaining redox reversibility at higher potential becomes critical during the battery operation. This high voltage operation coupled with electrolyte incompatibility can induce irreversible reactions, structural changes or degradation during charge and discharge cycles, which can result in capacity fading and reduced cycling stability. Therefore, enhancing stability and electrolyte compatibility of materials is required to ensure the long operation of p-type polymer cathodes in LIBs.

(ii) Low specific capacity: many p-type polymers exhibit lower specific capacities than traditional inorganic cathode materials due to their lower number of redox active sites. This lower specific capacity limits the energy density of LIBs utilizing p-type polymers as cathodes, impacting their overall performance and suitability for certain applications. Additionally, due to the fact that p-type polymers operate by incorporating anions from the electrolyte during the electrochemical process, the corresponding anions play an important role in defining their specific capacity. Furthermore, this anion involvement during electrochemical processes together with the instability of organic solvents in the electrolyte at high-voltage (>4.0 V) can result in the degradation and consumption of the electrolyte upon cycling, leading to a lower energy density. Consequently, providing more redox active sites in the polymer backbone through material design and electrolyte optimization is essential to enhance the storage capacity.

(iii) Minimum rate capability: the rate capability of p-type polymers refers to their ability to deliver and accept mobile ions at high charge and discharge rates. Some p-type polymers may exhibit a limited rate capability as a result of the slow ionic diffusion kinetics due to their poor electronic conductivity. Hence, enhancing the electronic conductivity of p-type polymer cathodes is crucial to provide rapid ion mobility during electrochemical processes.

(iv) Interfacial issues: the interface between the p-type polymer cathode and electrolyte plays a crucial role in ion transport and the overall battery performance. In batteries, poor electrolyte wetting properties, resistive electrode–electrolyte interphase, or unwanted interface reactions significantly hinder ion diffusion, and consequently decrease their efficiency. Therefore, addressing these interfacial issues is essential to improve the ion transport kinetics and enhance the performance of batteries.

(v) Electrode preparation issues: although polymer-based cathodes have minimum solubility in electrolytes, they often suffer from aggregation during electrode fabrication, thus reducing the effective surface area for ion transport and electrochemical reactions. This problem is worse in high-mass-loading electrodes, leading to an uneven current distribution, increased resistance, and reduced capacity. In large-scale preparation, their low electrical conductivity further hinder their performances. Therefore, the appropriate solvent selection and structural design are crucial for improving processability. Furthermore, the introduction of conductive additives such as carbon black, nanotubes, and graphene can enhance the electrical and ionic conductivity of polymer electrodes.

(vi) Cost and scalability: the production cost and scalability of p-type polymers are important considerations for their practical application in large-scale energy storage systems. Polymers with rare or expensive dopants, complex synthesis, and low processability may face challenges in cost-effective production and scalability, hindering their practical application and commercial viability. Therefore, developing cost-effective synthesis methods and utilizing abundant and sustainable raw materials are essential for realizing the widespread adoption of p-type polymer cathodes in LIBs and other energy storage devices.

3. Current progress in p-type polymer cathode materials

3.1 Polytriphenylamine

As a p-type compound, the structural specificity of the polytriphenylamine (**PTPA**) is recognized to originate from its radical nitrogen redox centers, which are stabilized by phenyl groups, facilitating radical redox reactions and charge-transporting processes. This structural feature allows high power capability and high energy density upon prolonged cycling. Additionally, its porous polymer structure with abundant interconnected holes due to its rigid phenyl groups provides sufficient surface area and ionic channels for rapid ion mobility.[117] Additionally, as a promising organic cathode material for LIBs, the redox activity of **PTPA** is attributed to the doping/de-doping process of anionic species on the nitrogen radical, providing a specific capacity of ~109 mA h g^{-1}.[62,88,118,119] However, some issues related to the low theoretical capacity, conductivity and processability of **PTPA**-based polymers still hinder their practical application. In this regard, Feng and coworkers reported simple **PTPA** (Fig. 3a) as an organic cathode material for LIBs.[120] The charge–discharge curves of the **PTPA** electrode exhibited an approximately linear relationship between voltage and capacity in the range of 4.2–3.6 V, resembling an electrochemical doping/de-doping process (Fig. 3b). At a moderate discharge rate of 0.5C, the discharge capacity reached 103 mA h g^{-1}, which is approximately 94% of the theoretical capacity of 109 mA h g^{-1}, but much lower than that of conventional electrodes, as shown in Fig. 3c.[120] Additionally, to enhance the specific capacity, the combination of different redox centers can facilitate greater electron transfer, and thus extend the storage capability. Similarly, Chen and colleagues successfully synthesized a novel micro-/mesoporous polymer, **PTDAPTz**, containing triazine units.[121] As shown in Fig. 3d, the energy gap between the lowest unoccupied molecular orbital (LUMO) and HOMO of **TDAPTz** was found to be stronger than that of **TPA** due to the stronger electron-withdrawing effect of the triazine unit, resulting in a lower band gap. This characteristic reflected in their electrochemical response as the redox peaks of the triphenylamine units in **PTDAPTz** shifted towards a higher potential than that of **PTPAn** (Fig. 3e) due to the electron-withdrawing effect of the triazine units, thus decreasing the electron cloud density nearby the nitrogen atom of triphenylamine and making it difficult to gain and lose the
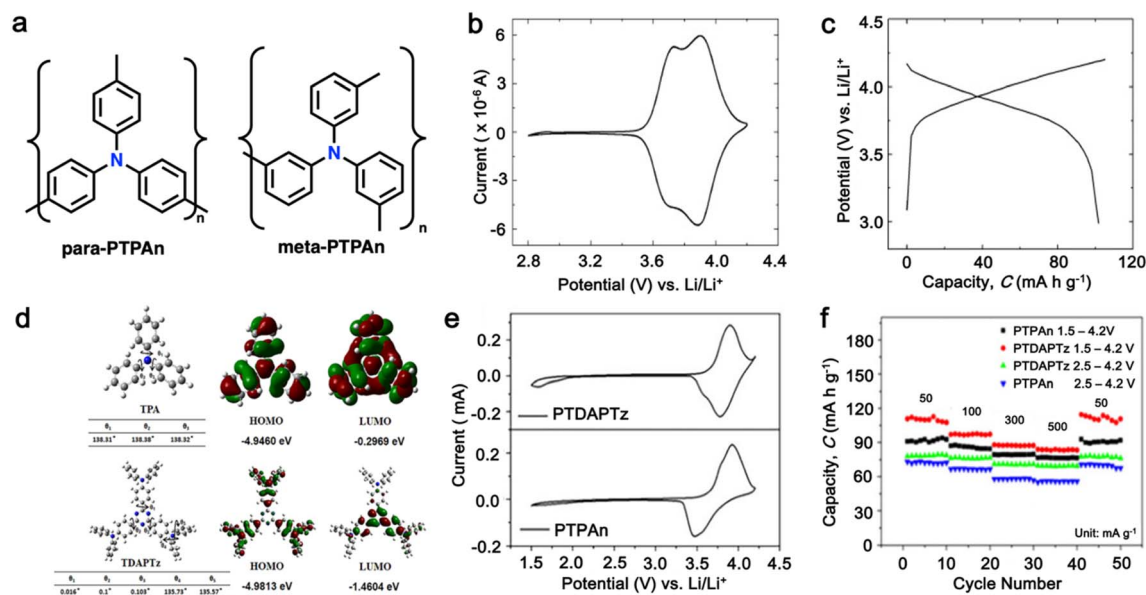
1558 | J. Mater. Chem. A, 2025, 13, 1552–1589

This journal is © The Royal Society of Chemistry 2025

Fig. 3 (a) Two possible isomers of **PTPAn**, (b) cyclic voltammetry (CV) curve of **PTPAn** in 1 M LiPF$_6$ EC/DMC (1 : 1 v/v) measured at a scan rate 1 mV s^{-1}, and (c) charge–discharge curves of Li-**PTPAn** test cells at a constant current of 50 mA g^{-1}. Reproduced with permission from ref. 120 Copyright 2008, Elsevier. (d) Molecular orbital (HOMO and LUMO) and geometric structure of **TPA** and **TDAPTz** monomers calculated theoretically using DFT calculation at the B3LYP/6-31G level performed using Gaussian 09. (e) CVs of **PTDAPTz** and **PTPAn** in 1 M LiPF$_6$ EC/DMC (v/v = 1 : 1) measured at 1 mV s^{-1} in the range of 1.5 of 4.2 V. (f) Rate performances of the **PTDAPTz** and **PTPAn** electrodes at various current rates. Reproduced with permission from ref. 121 Copyright 2018, John Wiley and Sons.

radical electron. This unique feature led to an improved cell performance, as shown in Fig. 3f. Furthermore, due to the high free radical density of the **PTPA** organic cathode, **PTDATA**, was synthesized to enhance the specific capacity via multiple electron transfer.[119] As shown in Fig. 4a, **PTDATA** exhibited multiple redox peaks compared to the **PTPA** cathode. These multiple peaks of **PTDATA** can be ascribed to the four free radical center structures in the **TDATA** unit of **PTDATA**, which undergo a four-electron transfer reaction during the charge–discharge process. These multi electron transfer successfully improved the cycling performance of the **PTDATA** cathode with the initial capacity of ~131 mA h g^{-1}, which was maintained at 98 mA h g^{-1} after 100 cycles at a current density of 20 mA g^{-1} (Fig. 4b).

Moreover, different strategies such as the formation of the hyperbranched and microporous **PTPA** polymer have also been applied to further improve the processability and structural stability of the electrode materials.[122,123] Yamamoto, et al. reported that hyperbranched phenylamine-based (**PHTPA**), prepared by Buchwald–Hartwig reaction (C–N coupling), exhibited high processability and delivered an ultrafast charge–discharge process (Fig. 4c).[122] The high processability of **PHTPA** was proven by the fact that it could easily dissolve in most of organic solvents such as N-methyl-2-pyrrolidone (NMP), THF, chloroform, and toluene although the polymer has all aromatic structures. Meanwhile, it remained insoluble in the electrolyte solution of 1 M LiPF$_6$ EC : DEC (30 : 70), indicating that **PHTPA** can be applied to LIBs. Furthermore, the **PHTPA** cathode delivered a stable specific capacity of ~60 and ~40 mA h g^{-1} at C rates of 20 and 100, respectively, up to 5000 cycles (Fig. 4c), demonstrating its ultralong stability and ultrafast charge–

discharge ability due to the formation of the microsphere morphology of the hyperbranched polymer.[122] Additionally, a star-shaped triphenylamine-based monomer with a benzene core was prepared to synthesize the conjugated microporous polymer poly[1,3,5-tris(4-diphenylamino-phenyl)benzene] (**PTTPAB**) via chemical oxidative polymerization (Fig. 4d).[123] This study found that the microporous structure is beneficial for providing fast ion transport, thus significantly improving the rate capability. As depicted in Fig. 4e, the **PTTPAB** cathode delivered a specific capacity of ~80 mA h g^{-1} without a significant capacity drop as the current density increased up to 500 mA g^{-1}.

In addition, copolymer formation has also been introduced in the **PTPA** organic cathode to improve its specific capacity. For instance, a novel conjugated radical copolymer, poly(triphenylamine-co-N,N′-bis(4-carbamoyl-2,2,5,5-tetramethyl-pyrrolin-1-oxyl)-N,N′ diphenyl-1,4-phenylenediamine) (**P(TPA-co-DDP-PROXYL)**), was synthesized through chemical oxidative polymerization and utilized as a cathode material.[124] This polymer incorporated both a crosslinking conjugated backbone and **PROXYL** nitroxide radical side chains. As shown in Fig. 4f, the presence of triphenylamine and nitroxide radicals within the polymeric backbone is expected to provide numerous active sites to improve the specific capacity. In this regard, a series of redox couples could be monitored in the CV profile of **P(TPA-co-DDP-PROXYL)** in the potential window of 2.5–4.2 V vs. Li/Li$^+$ (Fig. 4g). The two pairs of reversible redox peaks at 3.73/3.78 V (R1/O1) and 3.6/3.64 V (R2/O2) correspond to the para-substitution and meta-substitution redox reactions of the triphenylamine unit, respectively, while the R3/O3 (3.37/3.39 V) redox couple is associated
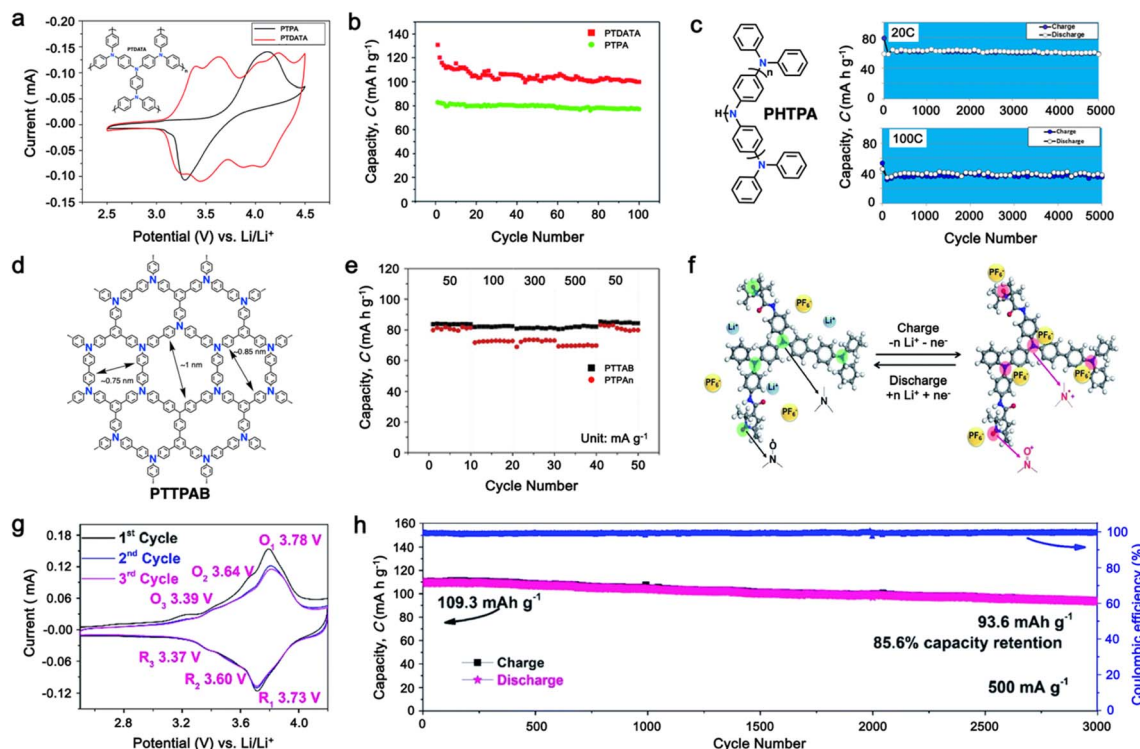
This journal is © The Royal Society of Chemistry 2025

J. Mater. Chem. A, 2025, 13, 1552–1589 | 1559

Fig. 4 (a) and (b) CV at a scan rate of 1 mV s^{-1} and cycling performance under a current density of 20 mA g^{-1} for the **PTDATA** cathode, respectively. Reproduced with permission from ref. 119 Copyright 2017, The Royal Society of Chemistry. (c) Chemical structure and cycling performance of hyperbranched **PHTPA** cathode at a high current rate. Reproduced with permission from ref. 122 Copyright 2018, the American Chemical Society. (d) and (e) Chemical structure and rate performance of microporous **PTTPAB** cathode. Reproduced with permission from ref. 123 Copyright 2018, Elsevier. (f) Schematic of electrochemical reaction mechanism of **P(TPA-co-DDP-PROXYL)**. (g) and (h) CV curve at a scan rate of 0.5 mV s^{-1} and long cycling performance of **P(TPA-co-DDP-PROXYL)** at 500 mA g^{-1}. Reproduced with permission from ref. 124 Copyright 2022, The Royal Society of Chemistry.

with the transition from the nitroxide radicals to the oxoammonium cations.[124] The resulting **P(TPA-co-DDP-PROXYL)** cathode material exhibited a superb electrochemical performance and ultralong cycle life with 72% capacity retention at 2000 mA g^{-1} over 3000 cycles (Fig. 4h).[124] This ultralong stability can be attributed to its rigid molecular structure and exceptional resistance when immersed in the electrolyte for extended periods. Moreover, Table 1 summarizes the recent development of phenylamine-based cathodes for organic LIBs. Overall, phenylamine-based electrodes have been explored and demonstrated superior high-rate capability, cycling stability, and energy density, making them promising cathode materials for next-generation organic LIBs operated at high voltage.

3.2 Thioether polymers

Organosulfur compounds have been recognized as potential cathode materials for LIBs due to their high theoretical capacity (1675 mA h g^{-1}) and energy density (2600 W h kg^{-1}) via the reversible formation/deformation of S–S bond formation.[28] However, despite their abundance and low cost, challenges such as their non-conductivity and the polysulfide shuttle effect limit their practical use.[133,134] Although organosulfur cathodes with diverse macromolecular structures can offer an improvement in stability and kinetics, some issues associated with S–S bond recovery have been encountered, thus impacting their

cycling stability.[135–137] Alternatively, thioether polymers, which are distinct from organosulfur compounds containing single S–S bonds, offer a different redox mechanism, involving the loss of electrons and formation of stable oxidation states.[138] This characteristic makes them potential candidates for cathodes with high voltage outputs, corresponding to the intercalation of anions (ClO$_4^-$, PF$_6^-$, BF$_4^-$, and TFSI$^-$).[139,140] Additionally, the charge storage mechanism of thioether polymers differs from organosulfur polymers, given that it does not involve chain breaking, potentially leading to higher cyclability.[141] Over the past few decades, numerous polymeric organosulfide materials have been developed, which can be categorized into four types including main-chain-type, side-chain-type, polysulfides with –S$_x$ groups where $x > 2$, and thioether-type organosulfur polymers.[134] Ren et al. synthesized two polyacetylene derivatives, **P1** and **P2**, containing pendant thianthrene groups through polymerization using the [(2,5-norbornadiene)RhCl]$_2$/Et$_3$N catalyst with thianthrene-1-ylmethyl 4-ethynylbenzoate (**M1**) or bis(thianthrene-1-ylmethyl)-4-ethynylphthalate (**M2**), as shown in Fig. 5a.[144] Both **P1** and **P2** exhibited reversible redox activity with a high oxidation potential of 4.16 V vs. Li/Li$^+$ due to the presence of p-type thioethers groups.[144] Notably, **P2** showed a higher specific capacity of 100 mA h g^{-1} compared to **P1** (33 mA h g^{-1}) (Fig. 5b and c), which is attributed to the more active units within the **P2** molecule. Moreover, adopting the

1560 | J. Mater. Chem. A, 2025, **13**, 1552–1589

This journal is © The Royal Society of Chemistry 2025

Table 1 Summary of the recent development of PTPA-based cathodes for organic LIBs
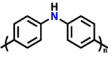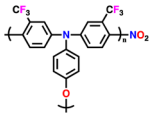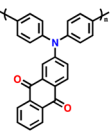
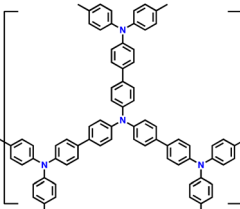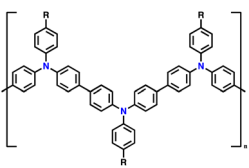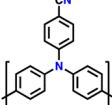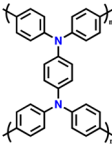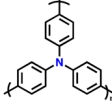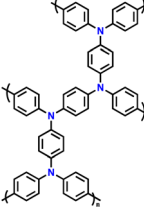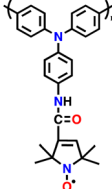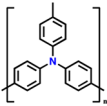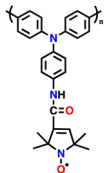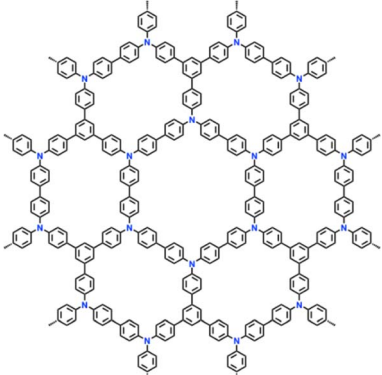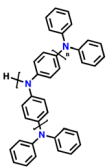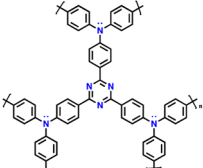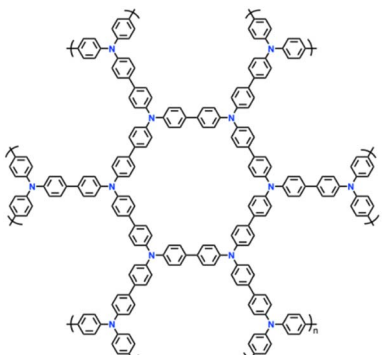| No.	Polymer material	Chemical structure	Electrolyte	Voltage (V) vs. Li/Li$^+$	Capacity (mA h g^{-1})	Current applied	Ref.
	Phenylamine-based cathodes						
1	**PDPA**		1 M LiPF$_6$ in EC/DMC (1 : 1, v/v)	2.5–4.5	116	0.1 A g^{-1}	125
2	**PTPA**		1 M LiPF$_6$ in EC/DMC (1 : 1, v/v)	2.5–4.2	69.7	0.05 A g^{-1}	126
4	**PDPA-AQ**		1 M LiPF$_6$ in EC/DMC (1 : 1, v/v)	1.5–4.5	159	0.1C	127
	PTPAn				100.4		
5			1 M LiPF$_6$ in EC/DMC (1 : 1, v/v)	2.5–4.2		0.02 A g^{-1}	128
	PTPA-CN				85.4		
6	**Poly(4-cyano) triphenylamine**		1 M LiPF$_6$ in EC/DMC/EMC (1 : 1 : 1, v/v/v)	3.0–4.2	75	0.08 A g^{-1}	129
7	**PDDP**		1 M LiPF$_6$ in EC/DMC (1 : 1, v/v)	2.5–4.2	110.6	0.02 A g^{-1}	88
8	**PTPA**		1 M LiPF$_6$ in EC/DMC (1 : 1, v/v)	2.5–4.2	80	0.02 A g^{-1}	88
9	**PFTP**		1 M LiPF$_6$ in EC/DMC (1 : 1, v/v)	2.5–4.2	74.2	0.02 A g^{-1}	130
10	**PTPA-PO**		1 M LiPF$_6$ in EC/DEC (1 : 1, v/v)	2.0–4.2	134.5	0.02 A g^{-1}	131

Table 1 (Contd.)

No.	Polymer material	Chemical structure	Electrolyte	Voltage (V) vs. Li/Li$^+$	Capacity (mA h g^{-1})	Current applied	Ref.
11	PTPA-CNT		1 M LiPF$_6$ in EC/DMC (1 : 1, v/v)	2–4.2	103.1	0.02 A g^{-1}	132
	PTPO-CNT				128		
12	PTTPAB		1 M LiPF$_6$ in EC/DMC/DEC (1 : 1 : 1, v/v/v)	2.5–4.2	86.5	0.02 A g^{-1}	123
13	PHTPA		1 M LiPF$_6$ in EC/DEC (3 : 7, v/v)	2.8–4.0	60	20C (1C = 0.06 A g^{-1})	122
14	PTDAPTz		1 M LiPF$_6$ in EC/DMC (1 : 1, v/v)	1.5–4.2	123	0.02 A g^{-1}	121
15	YPTPA		1 M LiPF$_6$ in EC/DMC (1 : 1, v/v)	2.5–4.2	100	0.1 A g^{-1}	87

same redox behavior, Vaid et al. reported a polythianthrene cathode with an impressive working potential of up to 4.1 V vs. Li/Li$^+$, which is comparable that of inorganic cathodes.[145]

Additionally, Misaki et al. demonstrated tris-fused tetrathiafulvalene (**TTF**) analogues, including unsubstituted- and bis(ethylenedioxy)-derivatives as cathode LIBs (Fig. 5d and e).[146]
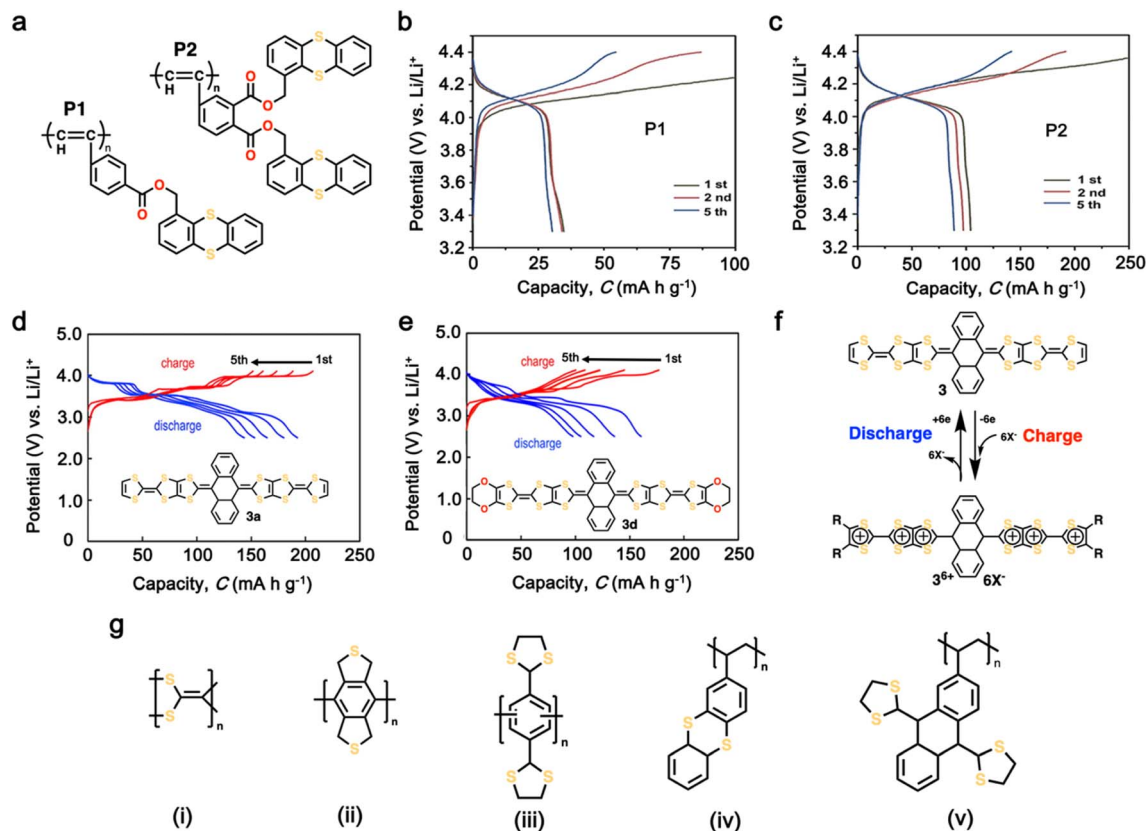
1562 | J. Mater. Chem. A, 2025, **13**, 1552–1589

This journal is © The Royal Society of Chemistry 2025

Fig. 5 (a) Chemical structure of polyacetylene derivatives containing thioether-based cathode, namely, **P1** and **P2**. (b) and (c) Charge–discharge profiles of thioether-based cathodes **P1** and **P2**. Reproduced with permission from ref. 142 Copyright 2020, Elsevier. (d) and (e) Charge–discharge profile and chemical structure of tetrathiafulvalene (TTF)-based cathode **3a** and **3d**, respectively. (f) Possible redox reaction of TTF-based cathode. Reproduced with permission from ref. 143 Copyright 2019, John Wiley and Sons. (g) Examples of representative p-type organosulfur polymers. Reproduced with permission from ref. 138.

As shown in Fig. 5d and e, these compounds delivered a voltage window of up to 3.6 V with a high capacity of 192 and 160 mA h g^{-1}. These distinct electrochemical performances were associated with the typical p-type reaction mechanism and six-electron electron transfer, as illustrated in Fig. 5f. However, these materials suffered from rapid capacity decay in the initial cycles, indicating the need to address their poor cycling stability (Fig. 5d and e). Furthermore, inspired by polymers, as presented in Fig. 5g(i and ii), polyphenyls with dithiolane moieties, as shown in Fig. 5g(iii), were prepared, showing promising stability and a stable capacity of up to 300 mA h g^{-1}.[147,148] However, these materials often exhibit large polarization due to their low conductivity, thus limiting their stability. Moreover, the incorporation of two sulfur atoms into a six-membered ring, as seen in thianthrene, results in exceptional stability.[149] Thianthrene-based polymers can lose two electrons alongside the intercalation of anions, leading to a high discharge plateau at around 4.0 V without a significant overpotential.[30] The Fig. 5g(iv) polymer exhibited highly reversible charge–discharge curves at 4.05 V for charging and 3.95 V for discharging, with a capacity of 105 mA h g^{-1} after the first cycle and 81% capacity retention after 250 cycles.[30] Employing a similar strategy, Schubert *et al.* utilized 1,3-dithiane in a five-membered ring polymer, which resulted in the discharge potential of about

3.2 V, where the charge storage mechanism involved anion intercalation (Fig. 5g (v)).[150] These findings highlight the potential of p-type thioether-based cathodes for high-potential LIBs, offering improved capacity, voltage, and cycle stability. Furthermore, Table 2 provides the recent trends in thioether-based cathodes for organic LIBs.

3.3 Dihydrophenazine-based polymers

In the preceding section, we explored how organic electrodes derived from triphenylamine-based polymers exhibit notably high redox potentials, though their specific capacities are typically around 100 mA h g^{-1}. This restriction arises from the fact that the triphenylamine unit tends to undergo a single-electron redox reaction, depending solely on a single nitrogen heteroatomic redox center on their polymer backbone. Thus, to overcome this limitation, recent studies have focused on developing p-type organic electrodes that are capable of multi-electron redox reactions to achieve higher capacities. In this regard, dihydrophenazine and its derivatives have been explored as new alternative p-type polymers with multi-electron redox reactions. These organic electrodes feature two heteroatomic redox centers (N, S, O) in their core six-membered ring, fused by two benzene rings, allowing two single-electron redox

This journal is © The Royal Society of Chemistry 2025

J. Mater. Chem. A, 2025, **13**, 1552–1589 | **1563**

Table 2 Summary of the recent development of thioether-based cathodes for organic LIBs

No.	Polymer material	Chemical structure	Electrolyte	Voltage (V) $vs.$ Li/Li$^+$	Capacity (mA h g^{-1})	Current applied	Ref.
	Thioether-based polymers						
1	**PPPS-14**		1 M LiTFSI in DOL/DME (1 : 1 v/v)	1.8–3.0	382.5	1C (1C = 0.622 A g^{-1})	151
2	Crosslinked polybenzenehexasulfide		1 M LiTFSI in DOL/DME (1 : 1 v/v)	0.75–3.2	150	0.1C	152
3	**PBDTD**		1 M LiClO$_4$ in DOL/DME (1 : 1 v/v)	1.9–3.2	180	5C (1C = 0.214 A g^{-1})	153
4	**PVBDT**		1 M LiClO$_4$ in EC/DMC (1 : 1 v/v)	1.5–3.25	116	1C	154
5	**PPTS**		1 M LiTFSI in DOL/DME (1 : 1 v/v) with 0.2 M LiNO$_3$	1.8–3.0	633	1C (1C = 0.778 A g^{-1})	155
6	**PBTTS**		1 M LiTFSI in DOL/DME (1 : 1 v/v) with 0.2 M LiNO$_3$	1.8–3.0	616.6	0.1C (1C = 0.901 A g^{-1})	156
7	**PEHS**		1 M LiTFSI in DOL/DME (1 : 1 v/v) with 0.2 M LiNO$_3$	1.8–3.0	774	1C (1C = 1.217 A g^{-1})	157
8	**S-BOP**		1 M LiTFSI in DIOX/TEGDME (0.67 : 0.33 v/v) with 0.2 M LiNO$_3$	1.7–2.7	630	1C (1C = 0.72 A g^{-1})	158
9	**S-TTCA**		1 M LiTFSI in DIOX/TEGDME (0.67 : 0.33 v/v) with 0.2 M LiNO$_3$	1.7–2.7	813	0.2C (1C = 1.675 A g^{-1})	159
10	**CP(S3BT)**		1 M LiTFSI in DOL/DME (1 : 1 v/v) with 0.1 M LiNO$_3$	1.5–3.0	682	1C	160

reactions and a significantly higher theoretical specific capacity (~270 mA h g^{-1}) than that of triphenylamine-based electrodes. The redox potentials of these phenazines are in the range of 3.1 to 4.2 V $vs.$ Li/Li$^+$ based on the electron-donating/withdrawing strength of the heteroatoms.

Among the phenazines, N,N'-substituted phenazine derivatives have captured interest due to their ability to undergo two successive one-electron transfer reactions, categorizing them as p-type molecules with higher redox potentials.[161] As shown in Fig. 6a, the reversibility of these electron transfer reactions depends on the substituted groups on the two N atoms. A

significant challenge in applying polymeric materials lies in their insufficient electrical and/or ionic conductivity, especially for those employing the anion-exchange mechanism.[22,165–167]

In this regard, Niu and colleagues explored manipulating the rigidity of polymer chains to alter the ion diffusion behavior in polymeric materials.[162] Their study revealed that introducing a suitable twisted group in phenazine-based polymers significantly enhances their ionic diffusion coefficient, leading to improved power densities despite their lower surface area and electrical conductivity.[168] This approach emphasized the different structural packing of the polymer chains, where the

1564 | *J. Mater. Chem. A*, 2025, **13**, 1552–1589
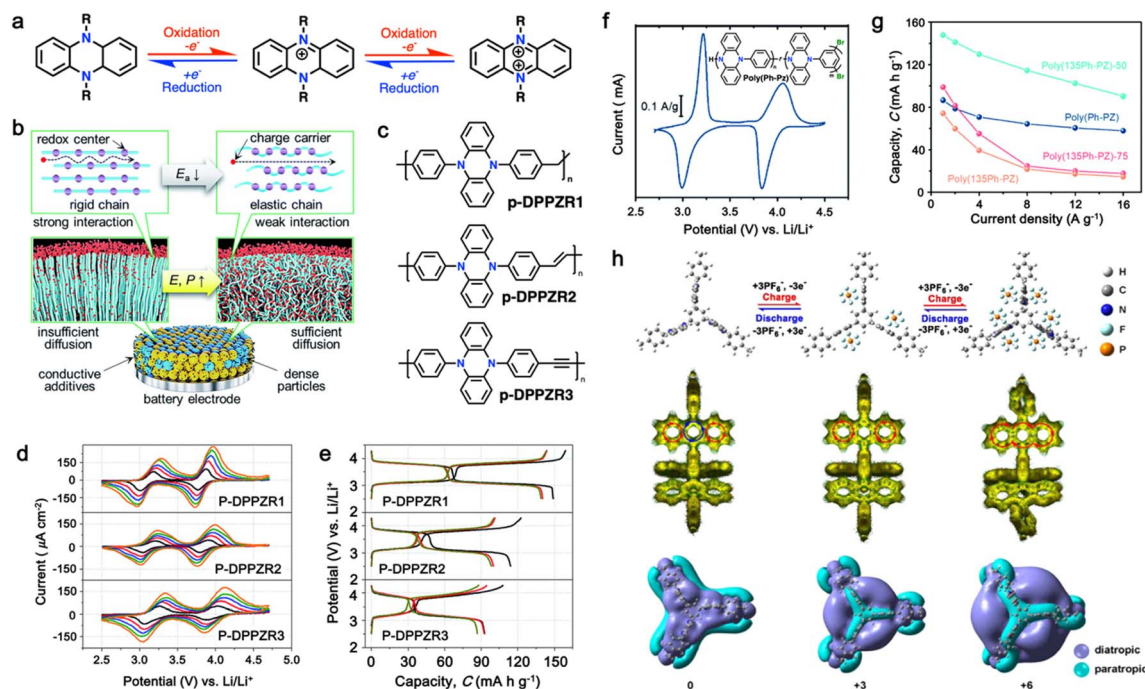
This journal is © The Royal Society of Chemistry 2025

Fig. 6 (a) Chemical structure and redox mechanism of N,N′-substituted phenazine derivatives. Reproduced with permission from ref. 84 Copyright 2019, Elsevier. (b) Schematic of enhancing the power density by decreasing the rigidity of the polymer chains. (c) Proposed polymers with variable chain rigidity based on DPPZ. (d) CV profiles of p-DPPZR1, p-DPPZR2, and p-DPPZR3 cells at sweeping rates of 0.2, 0.4, 0.6, 0.8, and 1 mV s^{-1}. (e) Typical charge/discharge profiles of p-DPPZR1, p-DPPZR2, and p-DPPZR3 at 1C rate. Reproduced with permission from ref. 162 Copyright 2019, The Royal Society of Chemistry. (f) CV profiles of poly(Ph-PZ) at 0.25 mV s^{-1} in Li metal half cells. (g) Rate capability of poly(Ph-PZ)-based cathode. Reproduced with permission from ref. 163 Copyright 2021, The Royal Society of Chemistry. (h) Redox mechanism and DFT calculation of TPZB cathode. Reproduced with permission from ref. 164 Copyright 2020, the American Chemical Society.

rigid chains often hinder ion diffusion through the polymer chain due to the increase in activation energy, while more elastic chains could accelerate the ion diffusion via the formation of an amorphous phase (Fig. 6b).[169,170] To validate this approach, three polymers based on redox-active N,N′-diphenyl-5,10-dihydrophenazine (DPPZ) were synthesized with varying chain rigidities, namely, p-DPPZR1 (–CH$_2$– bridging), p-DPPZR2 (–CH=CH– trans-isomer), and p-DPPZR3 (–C≡C–) (Fig. 6c).[162] As shown Fig. 6d, two pairs of redox peaks can be observed, corresponding to the two successive two-steps of one-electron redox reactions of DPPZ. In terms of specific capacity, p-DPPZR1 delivered a specific capacity of approximately 145.9 mA h g^{-1} (Fig. 6e), surpassing that of p-DPPZR2 (112.1 mA h g^{-1}) and p-DPPZR3 (93.7 mA h g^{-1}).[162] Additionally, to address the limitations posed by the strong π–π interactions narrowing the internal free volume, Gannett et al. developed a network polymer of PZ by incorporating a phenylene linker (Ph) with three points of connectivity, as shown in Fig. 6f.[163] This modification aimed to enhance the rate performance of the polymer system. Among the copolymers, poly(135Ph-PZ)-50 demonstrated the highest performance due to its optimal characteristics, as shown by the redox reactions in cyclic voltammetry (Fig. 6f). The polymer electrode achieved a specific capacity of up to 135 mA h g^{-1} at 1.0 A g^{-1}, retaining 65% of its low-rate capacity at a high rate of 16 A g^{-1} (Fig. 6g).[163] Furthermore, the optimized geometries of poly(1,3,5-tris(10-(4-

vinylphenyl)phenazin-5(10H)-yl)benzene) (TPZB) at the 0, +3, and +6 valence states were investigated, revealing the formation of a twist angle by the dihydrophenazine group with a centered benzene ring, creating storage space for PF$_6^-$ ions resembling piers (Fig. 6h).[164] This configuration facilitated their diffusion and intercalation/deintercalation. The calculation of iso-chemical shielding surfaces (ICSSs) further explored the aromaticity of the redox intermediates and their impact on the electrode performance (Fig. 6h).[164]

Additionally, substituting one of the N atoms with an S or O atom in the phenazine ring resulted in two further types of redox active compounds known as phenothiazine and phenoxazine, respectively. This substitution has been reported increase in the redox potential phenazine-based cathodes due to its weaker electron-donating strength. For instance, Kolek et al. introduced a phenothiazine (PTZ)-based polymer cathode, PVMPT, where N-methylated PTZ (MPT) units were attached to a vinyl backbone as pendant groups.[171] In this study, each MPT unit underwent two single-electron oxidations sequentially at 3.44 V (from neutral state A to radical cation state C) and 4.18 V vs. Li/Li$^+$ (to the di-cationic state D), respectively (Fig. 7a). Interestingly, as shown in Fig. 7b, the oxidation of PVMPT resulted in strong π–π interactions between neighboring MPT dimers, leading to the formation of the intermediate oxidation state at potentials of 3.44 and 4.18 V vs. Li/Li$^+$. Upon oxidation, the PTZ units in PVMPT could associate intra- or inter-
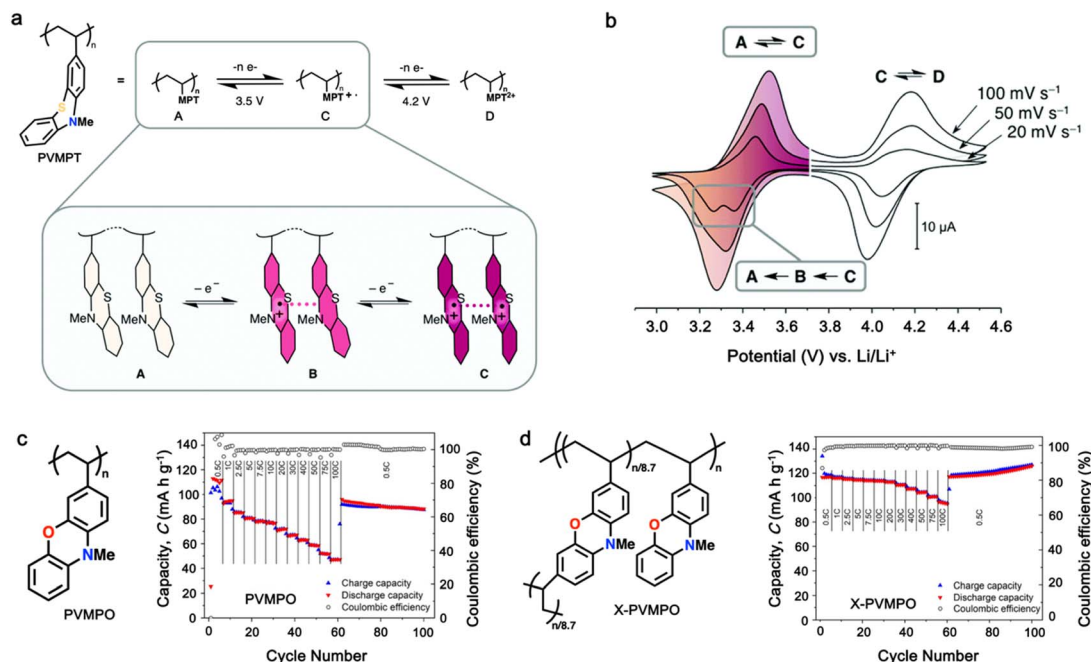
This journal is © The Royal Society of Chemistry 2025

J. Mater. Chem. A, 2025, 13, 1552–1589 | 1565

Fig. 7 (a) Schematic of the redox processes in **PVMPT** cathode. (b) Cyclic voltammograms of **PVMPT** in solution (1 mM in CH$_2$Cl$_2$, 0.1 M n-Bu$_4$NPF$_6$, glassy carbon working electrode). Reproduced with permission from ref. 171 Copyright 2017, The Royal Society of Chemistry. (c) Chemical structure and rate performance of **PVMPO** cathode. (d) Chemical structure and rate performance of **X-PVMPO** cathode. Reproduced with permission from ref. 172 Copyright 2020, The American Chemical Society.

molecularly, stabilizing oxidized states B and C, as depicted in Fig. 7b. These interactions became evident in the CV curves measured at a slow scan rate (20 mV s^{-1}), where the second cathodic peak, corresponding to the reduction of the radical cation to the neutral species (C → A), split into two peaks separated by 95 mV.[171]

Furthermore, phenoxazine (**PXZ**), a phenazine derivative, features an oxygen/nitrogen pair in its core ring and has been explored for cathode LIBs.[173] Otteny *et al.* replaced the **MPT** unit in the **PVMPT** polymer with *N*-methylphenoxazine (**MPO**) to create a poly(3-vinyl-*N*-methylphenoxazine) (**PVMPO**) polymer (Fig. 7c).[172] Showing similar electrochemical behavior to that of **PVMPT**, the **PVMPO** electrode exhibited two single-electron oxidation reactions at 3.35 and 4.22 V *vs.* Li/Li$^+$, although the second reaction was not entirely reversible. Notably, **PVMPO** displayed inferior cycle stability due to the lack of π–π interactions between the **MPO** dimers compared to that of **PVMPT**. Additionally, the cross-linked formation of **PVMPO** to form the **X-PVMPO** polymer (Fig. 7d) effectively enhanced the cycle stability by its preventing dissolution.[171,174] This strategy has significantly improved the cycling and rate capability performance of **PXZ**-based polymers. In addition, Table 3 illustrates the recent development of phenazine-based cathodes for organic LIBs.

3.4 Thianthrene and dibenzodioxin

Sharing a similar foundational structure with phenazine-based cathodes, thianthrene (**TT**) and dibenzodioxin (**DD**) have been considered next-generation high-voltage cathodes for LIBs by
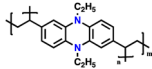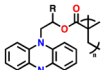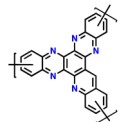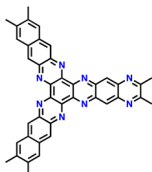
replacing nitrogen atoms with a sulfur atom (**TT**) and oxygen atom (**DD**), resulting in redox reactions at a higher voltage of ∼4.1 V. These heteroatoms play a vital role by providing multiple redox-active sites, enabling the essential multi-electron transfer reactions necessary for efficient charge and discharge processes in batteries. This characteristic is fundamental for achieving high specific capacities and ensuring a stable cycling performance, making both compounds highly attractive candidates for high-energy-density LIBs. A notable difference between **TT** and **DD** is the specific heteroatoms incorporated into their molecular structures. As shown in Fig. 8a, the redox mechanism of **TT**- and **DD**-based molecules demonstrates how each unit accommodates a single-electron transfer reaction. Recently, Speer and colleagues reported the preparation of three norbornene polymers, namely **P1**–**P3**, featuring one or two **TT** pendant groups as organic cathodes (Fig. 8b–d), respectively.[149] During the CV measurement, the first oxidation of the polymers showed a high redox potential (∼4.1 V *vs.* Li/Li$^+$), but the second one was irreversible for the **P2** polymer (Fig. 8b). Given that only one electron was utilized during the electrochemical process, their theoretical specific capacity was limited to 73 mA h g^{-1} and they practically delivered a specific capacity of ∼66 mA h g^{-1}, accounting for almost 90% of the total specific capacity. However, rapid decay over 100 cycles was observed due to irreversible anion intercalation (Fig. 8c). Importantly, the **P1** electrode still delivered a specific energy of 274 W h kg^{-1}, highlighting its promise for the preparation of high potential and high energy materials. Recently, Wild his group developed an all-organic battery consisting of

Table 3 Summary of the recent development of phenazine-based cathodes for organic LIBs

No.	Polymer material	Chemical structure	Electrolyte	Voltage (V) vs. Li/Li$^+$	Capacity (mA h g^{-1})	Current applied	Ref.
	Dihydrophenazine-based polymer						
1	**p-DPPZ**		1 M LiPF$_6$ in EC/DEC (1 : 1, v/v)	2.5–4.5	150	0.25C (1C = 0.209 A g^{-1})	84
2	**p-DPPZS**		1 M LiPF$_6$ EC/DEC	2.9–4.3	133	5C (1C = 0.147 A g^{-1})	175
3	**p-DPPZR-1**				140	1C (1C = 0.153 A g^{-1})	162
	p-DPPZR-2		1 M LiPF$_6$ in EC/DEC (1 : 1, v/v)	2.5–4.3	102	1C (1C = 0.148 A g^{-1})	
	p-DPPZR-3				88	1C (1C = 0.149 A g^{-1})	
4	**Poly(135Ph-PZ)**		1 M LiPF$_6$ in EC/DEC (1 : 1, v/v)	2.6–4.5	158	1 A g^{-1}	163
	Poly(135Ph-PZ)-X				180		
5	**Poly(Ph-PZ)**		1 M LiPF$_6$ in EC/DEC (1 : 1, v/v)	1.5–4.3	209	5C	176
6	**PBEMP**		1 M LiPF$_6$ in EC/DEC (1 : 1, v/v)	2–4.5	101	1 A g^{-1}	177
7	**p-TPPZ**		1 M LiPF$_6$ in EC/DEC (1 : 1, v/v)	2.5–4.5	171.9	0.5C (1C = 0.233 A g^{-1})	178
	p-DPPZ				169.7		
8	**PDPAPZ**		1 M LiPF$_6$ in EC/DMC	2.5–4.2	107	0.1 A g^{-1}	179
	PPTZPZ				83		
9	**p-TPZB**		1 M LiPF$_6$ in EC/DEC (1 : 1, v/v)	2.5–4.5	145	2C	164
10	**CPP**		1 M LiPF$_6$ in EC/DEC (1 : 1, v/v)	2.5–4.2	184	0.2 A g^{-1}	180
	NCPP				149		

This journal is © The Royal Society of Chemistry 2025

J. Mater. Chem. A, 2025, **13**, 1552–1589 | **1567**

Table 3 (*Contd.*)

No.	Polymer material	Chemical structure	Electrolyte	Voltage (V) vs. Li/Li$^+$	Capacity (mA h g^{-1})	Current applied	Ref.
11	R = Me, PMPPZ R = H, PMPEZ	R = Me, PMPPZ R = H, PMPEZ	1 M LiPF$_6$ in EC/DMC (1 : 1, v/v)	1.5–4.2	99 130	0.2 A g^{-1}	181
12	**HAT**		1 M LiPF$_6$ in EC/DMC (1 : 1, v/v)	1.0–3.5	99	10 A g^{-1}	182
13	**N^2-HATN**		LiCF$_3$SO$_3$ in G4	1.2–4.0	183	0.5 A g^{-1}	183

a poly(2-vinylthianthrene) cathode and poly(2-methacrylamide-TCAQ) anode.[185]

The cathode material of poly(2-vinylthianthrene) displayed a discharging plateau at 3.95 V *vs.* Li/Li$^+$ and a discharge capacity of 105 mA h g^{-1}, corresponding to a specific energy of about 415 mW h g^{-1}.

Despite their remarkable cell potential, **DD**-based cells suffered from severe capacity loss, reaching almost 50% during the first 10 cycles, due to the high solubility of **DD** molecules in the carbonate-based electrolytes system. In the early investigation of **DD**-based cathodes, Lee and group devised a modification strategy for a low-solubility **DD** analogue using a rigid iptycene scaffold to maximize the intermolecular interactions and form a **3D-DD** design incorporating three **DD**(CN)$_2$ units supported by the iptycene scaffold *via* facile nucleophilic aromatic substitution reactions (Fig. 8e).[92] The methyl-substituted quaternary carbon centers at the bridgehead positions prevented C–H activation reactions during the redox cycle. The stacked **3D-DD** structures were reported to form a complex structure by accommodating large lattice deformation through sliding motions of neighboring π-faces (Fig. 8f). Fig. 8g shows the voltage distribution of phenazine derivatives. As depicted in Fig. 8g, the **DD** electrode (blue line) displayed a redox peak at around 1.1 V *vs.* Ag/Ag$^+$, which is much higher than that of **PNZ** (orange line) or thianthrene (**TT**) (green line).[83,185] Notably, an increase in the redox potential of the **DD** molecules was achieved without the addition of any redox-inactive functional groups, which is generally accompanied by a reduction in the specific capacity.[186,187] Consequently, when oxygen atoms were introduced in the core structure, it showed a remarkable

increase in cell potential (4.1 V) against lithium, consequently delivering a discharge capacity of 90 mA h g^{-1} at 50 mA g^{-1} (Fig. 8h).[92] Besides the formation of a complex structure, different approaches have also been employed by incorporating conductive molecules. In this regard, Lee *et al.* synthesized a charge-transfer complex by combining **DD** with tetracyano-quinodimethane (**TCNQ**).[184] This **DD–TCNQ** complex demonstrated decreased solubility compared to the pristine **DD** and **TCNQ** molecules, which is attributed to the robust π–π interactions and coulombic attraction between their layers. Consequently, the **DD–TCNQ** electrode achieved a specific capacity of approximately 170 mA h g^{-1} at 50 mA g^{-1} within the voltage range of 2.6–4.2 V (Fig. 8i). The spectroscopic analysis unveiled that **DD** undergoes a single-electron redox reaction above the 4 V region, while **TCNQ** undergoes a two-electron redox reaction below the 4 V region during battery cycling. Throughout the charge and discharge process, it was hypothesized that the initial **DD–TCNQ** state transitions into **DD–LiTCNQ**, **DD–Li$_2$-TCNQ**, and **DD$^+$–TCNQ** (Fig. 8j). Their shared capability for multi-electron transfer reactions, coupled with the distinct advantages offered by their respective heteroatoms, underscores their potential for next-generation high-voltage cathodes. In brief, besides the **TT** and **DD**-based compounds capability of providing higher redox activity of > 4.0 V, addressing the related issue of high solubility due to solvent interaction and side reactions associated with C–S–C bond cleavage during cycling can pave the way for their practical application as LIB cathodes with enhanced energy density, extended cycle life, and improved overall performance. Moreover, Table 4 presents the recent advances in **TT** and **DD**-based cathodes for organic LIBs.
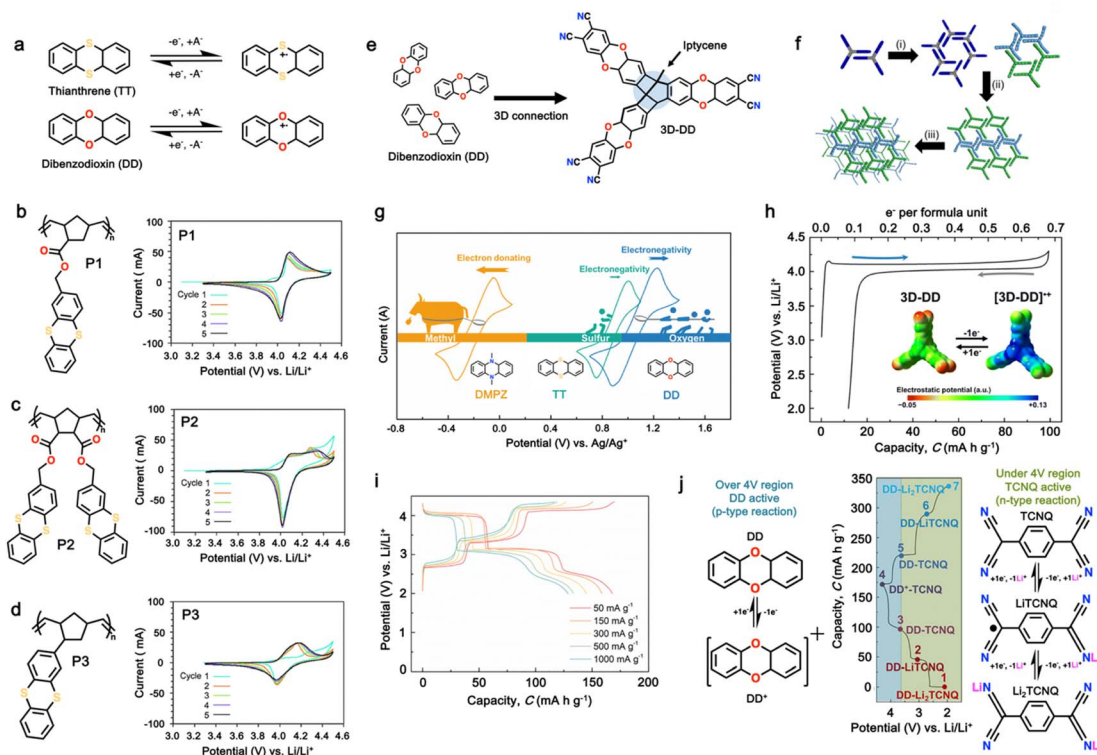
1568 | *J. Mater. Chem. A*, 2025, **13**, 1552–1589

This journal is © The Royal Society of Chemistry 2025

Fig. 8 (a) Redox mechanism of thianthrene (**TT**) and dibenzodioxin (**DD**). Chemical structure and cyclic voltammogram of **TT**-substituted polynorbornenes (b) **P1**, (c) **P2**, and (d) **P3**, respectively. Reproduced with permission from ref. 149 Copyright 2015, The Royal Society of Chemistry. (e) Schematic of the synthesis and (f) crystallographically determined solid-state structure of hyperjunction **3D-DD** cathode. (g) Cyclic voltammograms and the design scheme of **DMPZ**, **TT**, and **DD**. (h) Charge–discharge profiles of **3D-DD**. Inset figure shows MEP maps of **3D-DD** and [**3D-DD**]⁺ showing the charge delocalization over the three-blade components. Reproduced with permission from ref. 92 Copyright 2023, The Royal Society of Chemistry. (i) Rate capability of **DD–TCNQ** cathode. (j) Redox mechanism of **DD–TCNQ** cathode. Reproduced with permission from ref. 184 Copyright 2019, Elsevier.

3.5 Polyviologens

Polyviologens, also known as poly(4,4′-bipyridinium) compounds, are a class of organic materials that have gained significant attention for potential application in high-performance LIBs.[196–198] These materials as cathode LIBs are characterized by unique redox-active viologen units, which consist of an anion doping/de-doping process on two nitrogen-containing pyridinium rings connected by a conjugated bridge, leading to the formation of stable radical cations and dications.[190–194,199–201] Additionally, polyviologen-based cathodes offer several desirable properties for use in LIBs, including high electrochemical stability, good conductivity, and excellent cycling performance.[202] To further explore the potential of viologens, in 2015, Yao and colleagues introduced the first solid-type electrode based on viologen, presenting the viologen polymer poly(1,1′-pentyl-4,4′-bipyridinium dihexafluorophosphate (**PBPy**)), as shown in Fig. 9a (inset). The **PBPy** electrode exhibited two voltage plateaus at 2.6 and 2.1 V vs. Li/Li⁺, delivering a specific capacity of 79 mA h g⁻¹ in the initial cycle.[203] However, the low degree of polymerization led to rapid capacity degradation to 36 mA h g⁻¹ after 20 cycles. Nonetheless, when utilized as an anode, **PBPy** enabled the fabrication of an all-organic full-cell with poly(N-vinylcarbazole) (**PVK**) as the cathode, achieving a specific capacity

of 100 mA h g⁻¹ at a voltage of 1.8 V, relying on the PF₆⁻ anion charge carrier (Fig. 9a).[203] Furthermore, to improve the specific capacity and cycling performance, an anion insertion approach was reported to effectively increase the performance of viologen-based cathodes. For instance, Wang et al. reported the first Cl⁻-insertable p-type polymer, namely poly(butyl viologen dichloride) (**PBV-Cl₂**), as a cathode for LIBs (Fig. 9b).[190] As shown in Fig. 9c, **PBV-Cl₂** demonstrated a significant capacity improvement of up to 200 mA h g⁻¹ in the initial cycles compared to that of **PVB(PF₆)₂** at a current density of 50 mA g⁻¹. The improved specific capacity is associated with the presence of an inserted Cl⁻ ion in the structure, which contributed to the ion storage mechanism during the charge/discharge process. However, rapid capacity decay was observed during cycling in the first 50 cycles due to the dissolution of the **PBV-A₂** polymer in the carbonate-ether-based electrolyte and the inevitable anion exchange during the discharge–charge process (for **PBV-Br₂** and **PBV-Cl₂**).[190]

Similarly, a series of viologen-based cathodes was prepared to investigate the impact of the counter anion in the polymer structure.[191] As shown in Fig. 9d, poly(viologen halide)-based cationic polymers with Br⁻ and I⁻ as counter anions were prepared and nominated as **PVBVEtBr₂** and **PVBVEtI₂**, respectively. Notably, an additional redox peak appeared when the counter anions of Br⁻ and I⁻ were introduced in the viologen-

This journal is © The Royal Society of Chemistry 2025

J. Mater. Chem. A, 2025, **13**, 1552–1589 | **1569**

Table 4 Summary of the recent development of thianthrene, dibenzodioxin, and viologen-based cathodes for organic LIBs
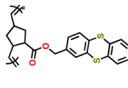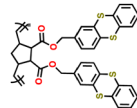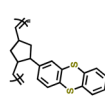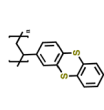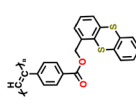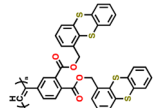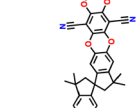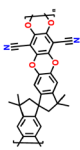
No.	Polymer material	Chemical structure	Electrolyte	Voltage (V) vs. Li/Li$^+$	Capacity (mA h g^{-1})	Current applied	Ref.
	Thianthrene-based polymers						
1	**P1**		1 M LiPF$_6$ in EC/DMC (1 : 1, v/v)	3.3–4.5	73	1C	149
2	**P2**		1 M LiClO$_4$ in EC/DMC (3 : 7 v/v)	3.2–4.2	105	1C	185
2	**Poly(2-vinylthianthrene)**				35		
3	**P1**		1 M LiPF$_6$ in EC/DMC (1 : 1, v/v)	3.3–4.4	100	0.05 mA cm^{-2}	144
3	**P2**						
	Dibenzodioxin-based polymers						
4	**PIM 1**		Dried PEO with LiTFSI (0.08 g) in 8 mL CH$_3$CN	1.6–2.7	1181	0.5C	188

1570 | J. Mater. Chem. A, 2025, **13**, 1552–1589

This journal is © The Royal Society of Chemistry 2025

Table 4 (*Contd.*)

No.	Polymer material	Chemical structure	Electrolyte	Voltage (V) vs. Li/Li$^+$	Capacity (mA h g^{-1})	Current applied	Ref.
	Polyviologen-based polymers						
5	PVPTOCl$_2$		1 M LiTFSI in (DOL:DME, 1:1 (v/v))	1.5–3.8	235	0.2 A g^{-1}	189
6	PVAQCl$_2$		1 M LiPF$_6$ in EC/DEC, (1:1, v/v)	1.4–3.1	113 / 177	0.2 A g^{-1}	190
7	PVBVEtX$_2$		2 M LiClO$_4$ in TEGDME	1.2–3.8	192	0.1 A g^{-1}	191
8	P-MV		1 M LiTFSI in DME	1.8–3.2	60	0.33C	192
9	PXVCl$_2$		0.5 M tributylmethylammonium chloride in propylene carbonate	1.5–3.2	140	0.01 A g^{-1}	193
10	EV(ClO$_4$)$_2$		2 M LiClO$_4$ in TEGDME	1.6–3.0	176 / 227	0.5C	194
	EVI$_2$						
11	POF		1 M LiPF$_6$ in EC/DMC (1:1, v/v)	1.5–4.5	130	3 A g^{-1}	195

This journal is © The Royal Society of Chemistry 2025

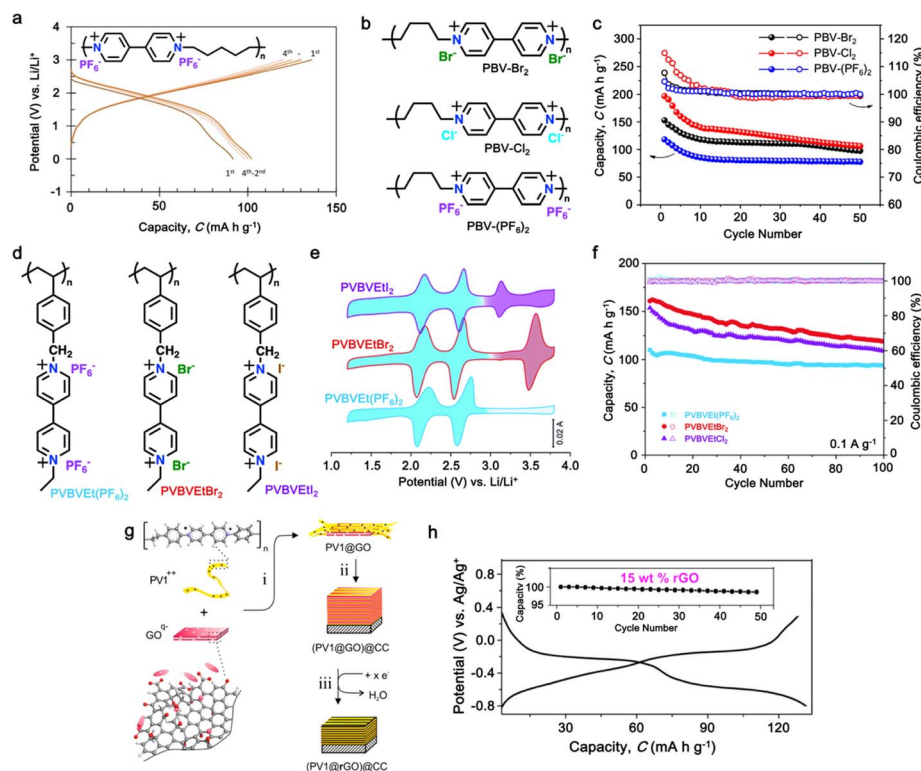*J. Mater. Chem. A*, 2025, **13**, 1552–1589 | **1571**

Fig. 9 (a) Galvanostatic charge–discharge profile of full-cell **PBPy**. Reproduced with permission from ref. 203 Copyright 2015, Springer Nature. (b) Chemical structure and (c) cycling performance under 50 mA g^{-1} in 1 M LiPF$_6$ EC : DEC electrolyte (voltage window of 1.4–3.1 V) of poly(butyl viologen)-based cathode. Reproduced with permission from ref. 190 Copyright 2022, Elsevier. (d) Chemical structures of viologen-based ionic polymers **PVBVEtX$_2$** (X = PF$_6^-$, Br$^-$ or I$^-$). (e) and (f) CV curves at 0.1 mV s^{-1} scan rate and cycling performance under 0.1 A g^{-1} current density of **PVBVEt(PF$_6$)$_2$**, **PVBVEtBr$_2$**, and **PVBVEtI$_2$** electrodes. Reproduced with permission from ref. 204 Copyright 2022, The Royal Society of Chemistry. (g) Overview of the preparation of poly-viologen/rGO composite electrode, **(PV1@rGO)@CC**. (h) Chronopotentiometric measurements of **(PV1@rGO)@GC** in 3 M KCl/H$_2$O at cutoff voltages in the range of 0.3–0.8 V, at a rate of 5 A g^{-1}. Reproduced with permission from ref. 199 Copyright 2017, The American Chemical Society.

based cathode. As shown in Fig. 9e, a strong and reversible redox peak was present at 3.53 V for **PVBVEtBr$_2$**, which can be assigned to the one-step reaction of the Br$^-$/Br$_3^-$ redox couple; while two redox peaks centered at 3.12 and 3.66 V were observed for **PVBVEtI$_2$**, corresponding to the oxidation of I$^-$ to I$_3^-$ (3.12 V), and then to I$_2$ (3.66 V). This involvement of the counter anion significantly improved the specific capacity of the viologen-based cathodes in the initial cycles, before gradually decaying up to 100 cycles (Fig. 9f). The capacity loss observed for the **PVBVEtBr$_2$** and **PVBVEtI$_2$** electrodes was mostly caused by the slight diffusion of Br$_3^-$, I$_3^-$ and I$_2$ species from the electrodes during the charge/discharge process.[191] In addition, it was reported that the formation of a composite electrode could improve the cycling stability of viologen-based polymers during the electrochemical process (Fig. 9g).[199] As shown Fig. 9h, the formation of a viologen-based polymer composite with 15 wt% reduced graphene oxide (rGO) significantly enhanced the cycling performance, given that negligible capacity loss was observed up to 50 cycles. Overall, the unique electrochemical properties and tunable structures of polyviologens make them promising candidates for the fabrication of high-performance LIBs and other energy storage technologies, with ongoing research aimed at further optimizing their performance and

expanding their applications in the future. Moreover, Table 4 shows the recent development of viologen-based cathodes for organic LIBs.

3.6 Nitroxide radical polymers

During the past decade, radical organic compounds have garnered significant attention in the realm of polymer-based batteries.[72,205–207] They feature polymers with pendant stable organic radicals, characterized by an unpaired electron in their uncharged state. These polymers offer superior redox chemistry with favorable kinetics, facilitated by redox reactions involving the singly occupied molecular orbital, enabling rapid electron transfer and high-rate performance capability. Considering the nonconjugated backbones and stable open-shell pendant groups of nitroxide radical polymers, they offer charge transport through a series of redox reactions between the pendant open-shell sites. Therefore, stable radicals such as nitroxyl, phenoxyl,[205,208] nitroxylbenzene,[209] nitronylnitroxyl,[210] and hydrazyl[211] groups, with structures such as 2,2,6,6-tetramethylpiperidine-*N*-oxy (**TEMPO**), have been explored as LIB cathodes.[207,212,213] Among the radical polymers, poly(2,2,6,6-tetramethylpiperidinyloxy-4-vinylmethacrylate) (**PTMA**)[54,166,214,215] and 2,2,6,6-tetramethyl-1-piperidinyloxy (**PTVE**)[213,216] have been
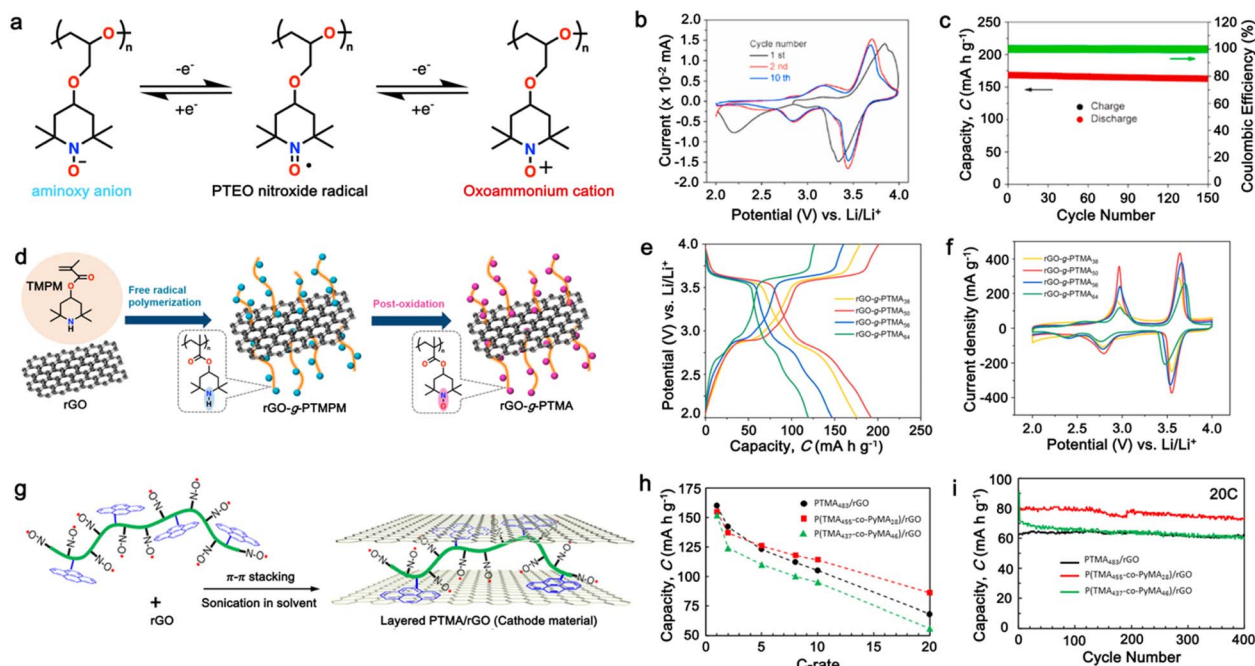
1572 | *J. Mater. Chem. A*, 2025, **13**, 1552–1589

This journal is © The Royal Society of Chemistry 2025

Fig. 10 (a) Electrochemical mechanism of **PTEO** nitroxide radical during charge/discharge cycles. (b) and (c) CV curves at a scan rate of 0.5 mV s⁻¹ and cycling performance under 1C rate (1C = 240 mA g⁻¹) of **PTEO** nitroxide radical, respectively. Reproduced with permission from ref. 217 Copyright 2020, Elsevier. (d) Schematic of the preparation of **PTMA**-grafted graphene sheets *via* free radical polymerization. (e) Galvanostatic charge−discharge curves (2nd cycle) under 1C and (f) CV curves of **rGO-*g*-PTMA** with different **PTMA** loadings. Reproduced with permission from ref. 218 Copyright 2021, Elsevier. (g) Formation of a layered **PTMA/rGO** composite through noncovalent π−π stacking between pyrene groups and **rGO** sheets. (h) and (i) Rate performance and cycling stability of layered **PTMA/rGO** composite, respectively. Reproduced with permission from ref. 219 Copyright 2017, the American Chemical Society.

investigated and showed high redox potentials of ∼3.6 V *vs.* Li/Li⁺. In this regard, a nitroxide radical polymer based on an ethylene oxide backbone, poly(4-glycidyloxy-2,2,6,6-tetramethylpiperidine-1-oxyl) (**PTEO**), was designed and reported (Fig. 10a). As shown in Fig. 10b, a two-step redox reaction of **PTEO** was observed in the CV curves, which is associated with the formation of the aminoxy anion at 2.75/3.20 V and oxoammonium cation at 3.48/3.60 V.[217] Due to the super high electrical conductivity of **PTEO** due to the unique open-shell site of the monomer and the completed conservation of all of the radical sites in the monomer, this PTEO delivered a specific capacity of 154 mA h g⁻¹ at a 1C rate after 150 cycles, corresponding to 91% capacity retention (Fig. 10c). Additionally, to improve the material stability and minimize the polymer solubility, Jin *et al.* grafted a **PTMA**-based polymer onto the surface of reduced graphene oxide (**rGO**) *via in situ* free radical polymerization (FRP), as shown in Fig. 10d. The electrochemical performance of **rGO-*g*-PTMA** showed that specific capacities ranging from 176 to 119 mA h g⁻¹ can be obtained at a current rate of 1C by varying the **PTMA** loading from 38 to 54 wt% (Fig. 10e). Notably, the **rGO-*g*-PTMA50** cathode exhibited the highest specific capacity. Moreover, CV measurement confirmed the electrochemical performance of **rGO-*g*-PTMA**, with the **rGO-*g*-PTMA50** sample demonstrating a superior performance, as shown in Fig. 10f.[218] Employing a similar approach, Zhang *et al.*[219] investigated a **PTMA**-based copolymer cathode combined with nanostructured carbon-based electrodes through non-covalent interactions (Fig. 10g). Prior to the addition of conductive carbon such as **rGO** and **CNTs**, ultrafast single electron transfer-nitroxide

radical coupling was applied to introduce pyrene groups in **PTMA**, forming **P(TEMPO-*co*-PyMA)** copolymers.

After that, the **P(TEMPO-*co*-PyMA)** copolymers were wrapped with **rGO** using ultrasonication and ultracentrifugation. Subsequently, these copolymers were bound to **rGO** flakes, forming electrode composites with a multilayered sandwich-like structure (Fig. 10g). This approach successfully enhanced the performance of the **PTMA**-based cathode, which delivered a high capacity of ∼150 mA h g⁻¹ at a 1C rate (Fig. 10h) and exhibited outstanding stability under a high current rate of 20C (Fig. 10i).[219] Table 5 describes the current trends in developing nitroxyl radical-based cathodes for organic batteries.

4. Alternative design of p-type polymer electrodes

4.1 Bipolar-type polymers

Bipolar-type polymers have emerged as promising candidates for next-generation high-performance LIBs due to their unique redox properties involving both p-type and n-type charge carriers, enabling the optimum charge storage and transport within the electrode material.[11] Due to the synergistic contribution of p- and n-type charge storage character, the nature of these polymers allows them to store and release both cations and anions during the charging and discharging processes, leading to enhanced energy storage capabilities.[22] This feature is particularly advantageous for achieving high specific capacities and energy density

This journal is © The Royal Society of Chemistry 2025

J. Mater. Chem. A, 2025, **13**, 1552–1589 | **1573**

**Table 5** Summary of the recent developments of nitroxide radical-based cathodes for organic LIBs
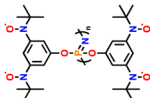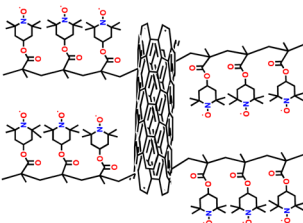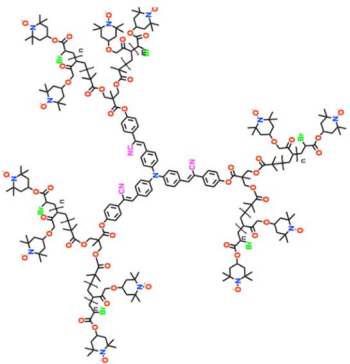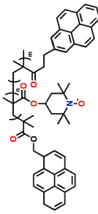
No.	Polymer material	Chemical structure	Electrolyte	Voltage (V) vs. Li/Li$^+$	Capacity (mA h g^{-1})	Current applied	Ref.
	Nitroxide radical-based polymers						
1	PNPP		1 M LiPF$_6$ in EC:DMC (1:1, v/v)	2.6–4.0	100	0.5C	220
2	PTMA-filled NCNT		1.2 M LiPF$_6$ in EC:DEC, (1:1, v/v)	1.5–4.0	159.6	1C	221
3	MWNT-g-PTMA		1 M LiPF$_6$ in (DMC:EC:EMC, 1:1:1 v/v/v)	2.0–4.0	243	1C (1C = 0.222 A g^{-1})	222
4	PTMA		1 M LiPF$_6$ in DMC	2.8–4.0	67	1C	223
5	PTEO		1 M LiPF$_6$ in PC	2.0–4.0	220	0.2C (1C = 0.24 A g^{-1})	217
6	PTMA		1 M LiPF$_6$ in EC:DMC, (1:1, v/v)	1.5–4.0	219,8 (2e$^-$) 110.9 (1e$^-$)	1C	224
7	PETM		1 M LiPF$_6$ in EC:DMC:EMC, (1:1:1 v/v/v)	3.0–4.2	90 (binder free) 99.5 (with PVDF)	10C	225

1574 | *J. Mater. Chem. A*, 2025, **13**, 1552–1589

This journal is © The Royal Society of Chemistry 2025

Table 5 (*Contd.*)

No.	Polymer material	Chemical structure	Electrolyte	Voltage (V) vs. Li/Li$^+$	Capacity (mA h g^{-1})	Current applied	Ref.
8	PTMA		1 M LiPF$_6$ in EC : DEC, (1 : 1, v/v)	3.0–4.2	32	0.025 mA	226
9	P(TMA-r-PyrM)		1 M LiPF$_6$ in EC : DEC, (1 : 1, v/v)	3.0–4.2	105	0.5C	227

in LIBs.[228] Bipolar-type polymers have demonstrated impressive electrochemical performance metrics in LIBs, including high specific capacities, excellent rate capabilities, and long-term cycling stability.[229] These polymers hold promise for a wide range of applications in portable electronics, electric vehicles, and grid energy storage systems, where high energy density, fast charging/discharging rates, and durability are critical requirements.[230] Recently, a series of bipolar polymers has been reported to significantly improve the specific capacity of LIBs. For instance, Zhang *et al.* reported two bipolar-type polymers by combining arylamine-based (p-type) and carbonyl-based (n-type) moieties to form poly(arylamine-imide)s, namely poly(*N,N,N′,N′*-tetraphenyl-1,4-benzenediamine naphthalenediimide) (**PDDP-NI**) and poly(*N,N,N′,N′*-tetraphenyl-1,4-benzenediamine perylenediimide) (**PDDP-PI**), as shown in Fig. 11a and b.[118] Bipolar activity was observed given that these polymers exhibited specific redox properties associated with their arylamine- and imide-units. As shown in Fig. 11a and b, both **PDDP-NI** and **PDDP-PI** exhibited three pairs redox peaks at ~2.46/2.30, 3.56/3.44, and 3.98/3.87 V, respectively. The first pair redox peak is ascribed to the redox activity of the carbonyl group in the imide unit (n-type), while the other two redox couples are associated with the doping/de-doping process of the arylamine unit (p-type). Furthermore, this strategy successfully improved the cathode specific capacity up to 150.9 (**PDDP-NI**) and 119.4 (**PDDP-PI**) mA h g^{-1} after 70 cycles at 0.1C.

Employing a similar approach, a series of bipolar triphenylamine-based polynaphthalimides (**TPA-PNIs**) was reported not only as a cathode, but also as an anode and binder-free cathode in LIBs.[62] These **TPA-PNI** cathodes delivered a high specific capacity of up to 195 mA h g^{-1} after 100 cycles at 50 mA g^{-1} due to the synergistic contribution from both the p- and n-type units. As shown in Fig. 11c, these polymers exhibited outstanding stability up to 5000 cycles under an extreme current density of 2000 mA g^{-1}. Notably, no significant capacity drop was observed even as a binder-free cathode (Fig. 11c), suggesting the excellent material stability and dual-role ability as active materials and electrode binder simultaneously. In another study, Labasan *et al.* developed two polyimide (PI) derivatives, **TPA-PMPI** and **TPA-NTCPI**, as electrode materials for LIBs.[58] These polymers exhibited excellent thermal stability and bipolar properties. The **TPA-NTCPI** cathode delivered a reversible specific capacity of 150 mA h g^{-1} at 0.1 A g^{-1} and showed stability up to 1000 cycles, while the **TPA-PMPI** anode achieved a high specific capacity of up to 1600 mA h g^{-1} at 0.1 A g^{-1} after 100 cycles.[58] Furthermore, various polymerization methods have also been studied to integrate bipolar moieties. Wang and colleagues successfully polymerized amino-phenyl carbazole naphthalene diimide (**APCNDI**) using *in situ* electropolymerization to eliminate the dissolution problem.[233] The electropolymerized cathode demonstrated an excellent electrochemical performance, stable cycling performance, and superior rate performance. In addition, employing a different strategy, Zhao and colleagues integrated a series of n- and p-type redox-active moieties into one stable polymer backbone to minimize the redox-inactive moieties (Fig. 11d).[232] As shown in Fig. 11e, the CV curves of **P-BQPZ** demonstrate clear and
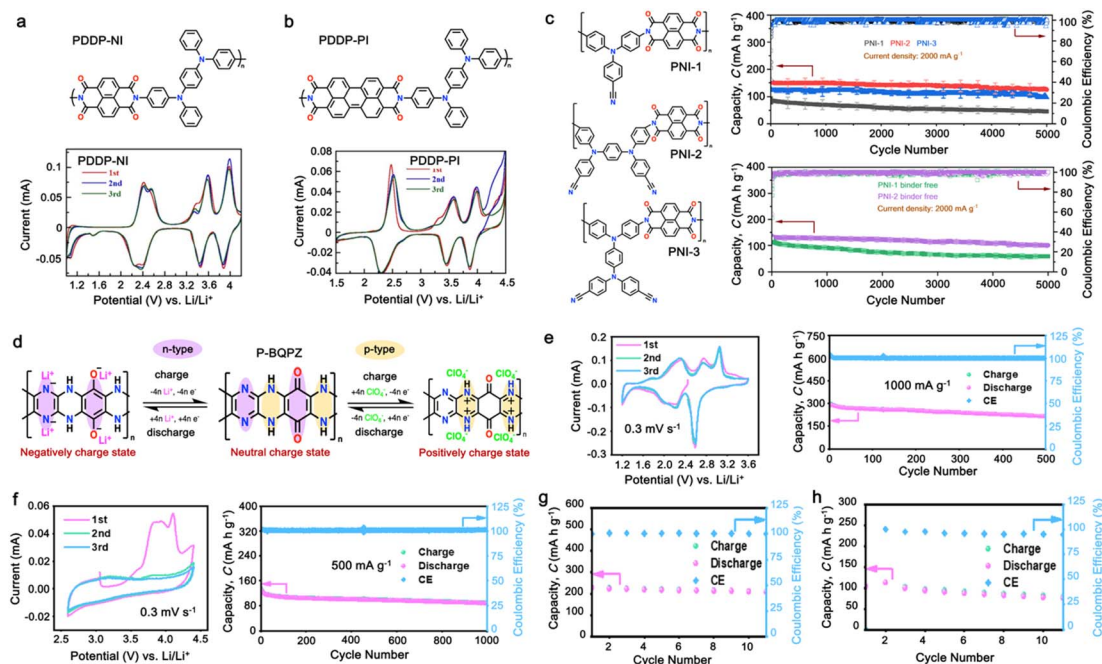
This journal is © The Royal Society of Chemistry 2025

J. Mater. Chem. A, 2025, **13**, 1552–1589 | **1575**

Fig. 11 (a) and (b) Chemical structure and cyclic voltammogram of **PDDP-NI** and **PDDP-PI** bipolar polymer, respectively. Reproduced with permission from ref. 231 Copyright 2021, The Electrochemical Society. (c) Chemical structures and long cycling performance of redox-active polynaphthalimides (**PNIs**). Reproduced with permission from ref. 62 Copyright 2023, The Royal Society of Chemistry. (d) Chemical structure and redox reaction mechanism of the bipolar polymer **P-BQPZ**. (e) and (f) CV curves and long cycling performance of n-type **P-BQPZ** and p-type **P-BQPZ**, respectively. (g) Cycling performance of the full cell based on n-type redox reaction of **P-BQPZ** at a current of 500 mA g^{-1} between 0.1 and 2.7 V. (h) Cycling performance of the full cell based on p-type redox reaction of **P-BQPZ** at current of 50 mA g^{-1} between 0.1 and 3.4 V. Reproduced with permission from ref. 232 Copyright 2022, Elsevier.

reversible redox peaks of n-type redox reactions, which are attributed to the C=O bond at 2.6, 2.7, and 3.0 V (*vs.* Li/Li$^+$) and C=N bond at 2.3 and 2.2 V (*vs.* Li/Li$^+$). This redox activity contributed to the specific capacity of 213.3 mA h g^{-1} up to 500 cycles at a current density of 1000 mA g^{-1} (Fig. 11e). Additionally, the activity of the **P-BQPZ** p-type cathode is depicted in Fig. 11f, showing higher redox activity at 3.1 V (*vs.* Li/Li$^+$) and contributing a capacity of ~120 mA h g^{-1} up to 1000 cycles at 500 mA h g^{-1}. Additionally, the cycling performance of the full cell based on the n-type and p-type redox reaction of **P-BQPZ** is presented in Fig. 11g and h, respectively, depicting the successful incorporation of **P-BQPZ** in the full cell LIB system. These findings provide a novel strategy for designing and fabricating high-performance cathode LIBs by combining two different electrochemical characters, thus offering potential solutions to improve the energy density. Continued research efforts are aimed at advancing the synthesis, characterization, and understanding of these polymers as well as their minimizing synthetic cost, which are essential for realizing their full potential in energy storage applications. Furthermore, Table 6 describes the current trends in developing alternative designed p-type cathodes for organic batteries.

4.2 Hybrid organic–inorganic polymers

Hybrid organic–inorganic polymers have emerged as promising alternatives to improve the electrochemical performance and stability of polymer-based electrodes. This synergistic combination of both organic and inorganic character offers opportunities to overcome the limitations associated with conventional electrode materials and develop high-performance LIBs with enhanced energy storage capabilities. One common approach in designing organic–inorganic hybrid electrodes involves incorporating a polymer matrix into the structure of inorganic materials. For example, organic molecules such as conducting polymers, viologens, and redox-active organic compounds can be integrated with inorganic materials such as metal oxides, sulfides, phosphides, and carbon-based materials to form hybrid electrode composites.[254] These composites exhibit improved electrochemical properties, including high capacity, cycling stability, and rate capability, compared to their individual components. Another strategy involves the synthesis of nanostructured hybrid materials, where organic and inorganic components are intimately intertwined at the nanoscale. This approach enables precise control of the morphology, surface area, and interfacial properties of the electrode materials, leading to enhanced ion diffusion kinetics and electrochemical performance.[255] Nanostructured hybrid materials can be fabricated using techniques such as sol–gel synthesis, hydrothermal synthesis, chemical vapor deposition, and electrodeposition.[256]

Several types of organic–inorganic hybrid materials have been investigated for LIB electrodes, including metal–organic frameworks (MOFs),[255,257,258] covalent organic frameworks (COFs),[53,65,259–261] conductive polymers/carbon composites,[262,263] and redox-active organic–inorganic composites.[264,265] In

1576 | *J. Mater. Chem. A*, 2025, **13**, 1552–1589

This journal is © The Royal Society of Chemistry 2025

Table 6 Summary of the recent development of alternative designs of p-type cathodes for organic LIBs
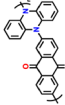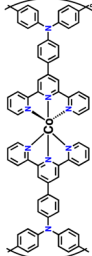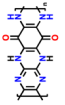
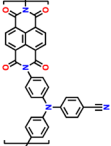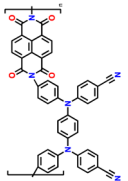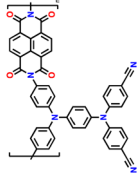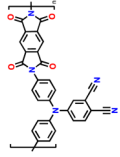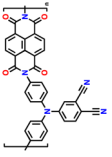| No.	Polymer material	Chemical structure	Electrolyte	Voltage (V) vs. Li/Li$^+$	Capacity (mA h g^{-1})	Current applied	Ref.
	Bipolar-type polymers						
1	PAQDPZ		3 M LiFSI in TEGDME	1.6–4.3	105 (symmetric organic battery)	0.2 A g^{-1}	234
			1 M LiPF$_6$ in EC/DEC	1.5–4.2	208 (Li-ion full cell)	0.2 A g^{-1}	
			3 M LiFSI in TEGDME	1.6–4.3	222 (Li-ion half-cell)	0.2 A g^{-1}	
2	Poly(CoL)$_n$		1 M LiPF$_6$ in EC : DEC, (1 : 1, v/v)	1.5–4.5	125.16	2 A g^{-1}	235
3	P-BQPZ		1 M LiTFSI in DOL : DME (1 : 1, v/v)	2.6–4.4	130 (p-type)	0.5 A g^{-1}	232
			1 M LiClO$_4$ in EC : DMC (1 : 1, v/v)	1.2–3.6	298 (n-type)	1 A g^{-1}	
	PNI-1				125		
4	PNI-2		1 M LiPF$_6$ in EC : DEC (1 : 1, v/v)	1.5–4.5	195	0.05 A g^{-1}	62
	PNI-3				170		
5	DAAQ		1 M LiPF$_6$ in EC : DMC (1 : 1, v/v)	1.5–4.5	311	0.05 A g^{-1}	236
6	TPA-PMPI		1 M LiTFSI in DOL : DME (1 : 1, v/v)	1.5–3.5 (cathode)	150	0.1 A g^{-1}	58
	TPA-NTCPI						

This journal is © The Royal Society of Chemistry 2025
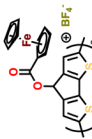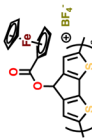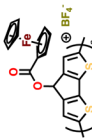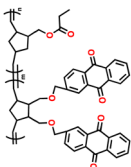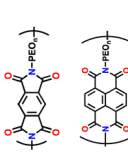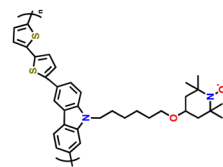
J. Mater. Chem. A, 2025, **13**, 1552–1589 | **1577**

Table 6 (Contd.)

No.	Polymer material	Chemical structure	Electrolyte	Voltage (V) vs. Li/Li$^+$	Capacity (mAh g^{-1})	Current applied	Ref.
	Hybrid organic–inorganic polymer						
7	LiV$_3$O$_8$/polythiophene (LiV$_3$O$_8$/PTh)		1 M LiPF$_6$ in EC : DMC (1 : 1, v/v)	1.8–4.0	213.3	1C (1C = 0.3 A g^{-1})	237
8	LiV$_3$O$_8$/polydiphenylamine		1 M LiPF$_6$ in EC : DMC : EMC, (1 : 1 : 1, v/v/v)	1.8–4.0	311	0.06 A g^{-1}	238
	pCPDT-Fc **P1**				59.7	0.1C (1C = 0.066 A g^{-1})	239
9			1 M LiPF$_6$ in EC : DMC (1 : 1, v/v)	2.7–3.9			
	pDTP-Fc **P2**				59.8		
10	NMC/PPy		1 M LiPF$_6$ in EC : DMC : EMC, (1 : 1 : 1 (v/v/v)	2.5–4.5	202.2	0.2C	240
11	LMNC@Li$_3$PO$_4$&PANI		1 M LiPF$_6$ in EC : DMC : EMC, (1 : 1 : 1) (v/v/v)	2.0–4.8	172.60	1C	241
12	Li$_{1.2}$Ni$_{0.2}$Mn$_{0.6}$O$_2$/PEDOT:PSS		1 M LiPF$_6$ in EC : DMC (1 : 1, v/v)	2.0–4.8	285	0.2C (1C = 0.3 A g^{-1})	242
	Copolymer materials						
13			2 M LiTFSI in DOL/DME (1 : 1, v/v)	1.5–3.0	127 / 84	0.1C / 1C (1C = 0.172 A g^{-1})	243
14	Pyromellitic polyimide-*b*-PEO		1 M LiTFSI/MeTHF	1.0–3.4	225 / 160	1.1C (1C = 0.203 A g^{-1})	244
15	**pBTC-TEMPO**		1 M LiPF$_6$ in EC/DMC, (1 : 1, v/v)	3.0–4.0	50	1C (1C = 0.06 A g^{-1})	245
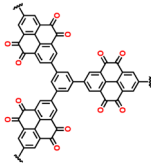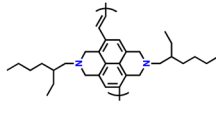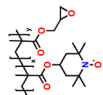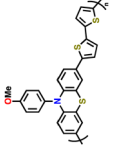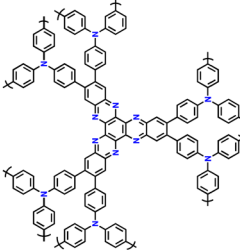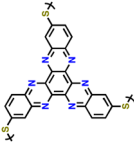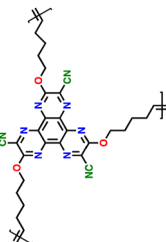
1578 | J. Mater. Chem. A, 2025, **13**, 1552–1589

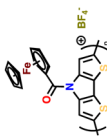This journal is © The Royal Society of Chemistry 2025

Table 6 (*Contd.*)

No.	Polymer material	Chemical structure	Electrolyte	Voltage (V) vs. Li/Li$^+$	Capacity (mAh g^{-1})	Current applied	Ref.
16	**Poly-PPDA-PYR**		1 M LiPF$_6$ in EC/DMC, (1:1, v/v)	2.0–4.2	75	0.5 A g^{-1}	246
17	**PPh-PTO**		1 M LiTFSI in DOL/DME (1:1, v/v)	1.5–3.8	235	0.1 A g^{-1}	247
18	**PENDI**		1 M LiPF$_6$ in EC/DMC, (1:1, v/v)	1.0–4.0	110	0.1C (1C = 0.202 A g^{-1})	248
19	**PTMA-*co*-GMA**		1 M LiPF$_6$ in EC/DEC (1:1, v/v)	3.0–4.0	104	0.1C	249
20	***p*(APT-T2)**		1 M LiPF$_6$ in EC/DMC (1:1, v/v)	3.2–4.2	68.5	1C	250
21	**PTPA-HATN**				120		
	PDTPA-HATN		1 M LiPF$_6$ in EC/DMC/EMC (1:1:1, v/v/v)	1.5–4.2	103.6	0.025 A g^{-1}	251

This journal is © The Royal Society of Chemistry 2025

J. Mater. Chem. A, 2025, **13**, 1552–1589 | **1579**

Table 6 (Contd.)

No.	Polymer material	Chemical structure	Electrolyte	Voltage (V) vs. Li/Li$^+$	Capacity (mA h g^{-1})	Current applied	Ref.
22	NSHATN		LiCF$_3$SO$_3$ in G4	1.5–4.0	337	0.05 A g^{-1}	252
23	HATCNOC-poly		1 M LiTFSI in TEGDME	1.0–2.8	158.6	0.05 A g^{-1}	253

particular, Zhu *et al.* developed a composite cathode material by introducing polydiphenylamine (**PDPA**) in the lithium trivanadate (LiV$_3$O$_8$, **LVO**) using an *in situ* oxidative polymerization method, leading to significant improvements in electrochemical properties and the inhibition of adverse reactions, as shown i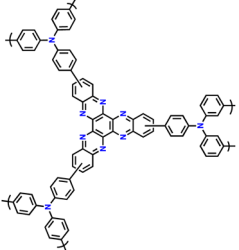n Fig. 12a.[238] The TEM analysis revealed that the surfaces of LiV$_3$O$_8$ were coated with a layer of **PDPA**, with an average polymer thickness of around 20 nm (Fig. 12b). The 10 wt% LiV$_3$O$_8$/**PDPA** composite exhibited a high initial specific discharge capacity of 311 mA h g^{-1}, which decreased to 272 mA h g^{-1} after 50 cycles at a current density of 60 mA g^{-1}. Furthermore, the composite displayed a remarkable improvement in rate capability, with its discharge capacities at various current densities outperforming that of the pure **LVO** electrodes (Fig. 12c). This increased performance of the **LVO**-based cathode could be ascribed to its high conductive coating of **PDPA**. With a similar aim, LiFePO$_4$/poly(3,4-ethylenedioxythiophene) (**PEDOT**) composites were prepared.[267] Furthermore, poly(aniline) was also explored to coat an LiFePO$_4$ cathode, resulting in a hybrid polymer–inorganic composite. It was demonstrated that the polymer not only served as a conductive matrix and binder but also as an additional host for lithium-ion intercalation. At a 0.2C rate, it achieved a capacity of 165 mA h g^{-1}, which decreased by 25% to 123 mA h g^{-1} at a 10C rate. Despite this, the discharging curves remained flat, suggesting its good cycling stability.[268]

In addition, a triphenylamine-based MOF, **Cu-TCA** (**H$_3$TCA** = tricarboxytriphenyl amine), was reported as a LIB cathode active material.[269] In this framework architecture, the redox activity of **Cu-TCA** is associated with the redox activity of both the metal clusters (Cu^{+}/Cu^{2+}) and organic ligand radicals (N/N$^+$) with separated voltage plateaus and a high working potential of up to 4.3 V (*vs.* Li/Li$^+$). Due to its abundant redox-active constituents and highly stable organic ligands, **Cu-TCA** has a theoretical capacity of 145 mA h g^{-1}, which is comparable to that of commercial materials such as LiFePO$_4$ (170 mA h g^{-1}). Moreover, **Cu-TCA** achieved long cycling stability over 200 cycles at a 2C rate, with an average coulombic efficiency of 96.5%, suggesting that **Cu-TCA** is capable of delivering a high recharge rate with high-capacity retention. Inspired by these findings, Lin *et al.* explored the potential of nitroxide radical-based **PTMA** as a cathode material (Fig. 12d) by polymerizing a polymer brush over silica nanoparticles.[266] The nitroxide polymer brushes, grafted onto silica nanoparticles *via* surface-initiated atom transfer radical polymerization, prevented the dissolution of the polymer in organic electrolytes. The SEM and TEM images confirmed that the nitroxide polymer brushes were successfully grafted onto the silica nanoparticles (Fig. 12e and f). Further, the electrochemical quartz crystal microbalance results indicated that the non-crosslinking nitroxide polymer brushes prevented the polymer from dissolving in organic electrolytes (Fig. 12g). These electrodes showed high discharge capacities and excellent cycle-life performance, demonstrating the potential of organic–inorganic hybrid systems for energy storage applications. Similarly, Schwartz *et al.* synthesized conjugated polymers based on ferrocene-functionalized cyclopentadithiophene and poly(dithieno[3,2-*b*:2′,3′-*d*]pyrrole) backbones (Fig. 12h).[239] These polymers exhibited high reversible capacities and excellent
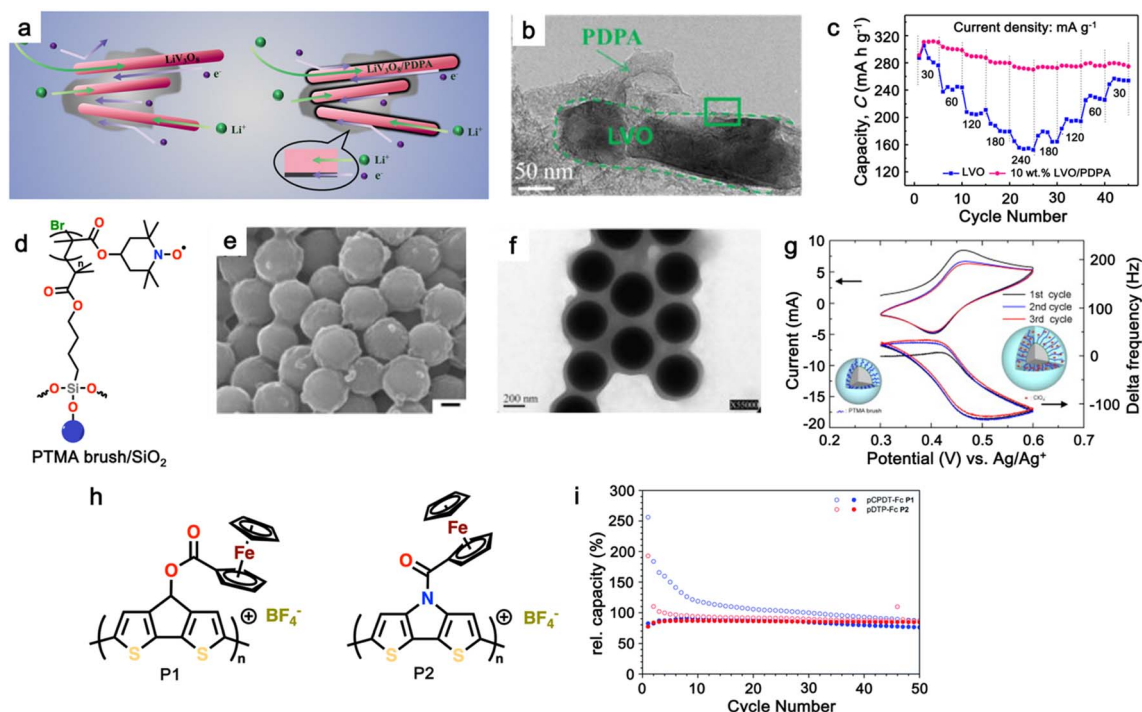
1580 | *J. Mater. Chem. A*, 2025, **13**, 1552–1589

This journal is © The Royal Society of Chemistry 2025

Fig. 12 (a) Schematic depicting the Li⁺ and electron-transfer pathway for **LVO** and **LVO/PDPA** composites. (b) TEM micrographs showing the morphology of 10 wt% **LVO/PDPA** composite. (c) Comparison of the rate capabilities between **LVO** and 10 wt% **LVO/PDPA** composites at various current densities. Reproduced with permission from ref. 238 Copyright 2018, the American Chemical Society. (d) Chemical structure of **PTMA** brush/SiO_2 hybrid materials. (e) and (f) SEM and TEM images of **PTMA** brush/SiO_2, respectively. (g) Cyclic voltammogram of **PTMA** brush/SiO_2 on the Au electrode and its corresponding resonance frequency change in EQCM sensor. The electrolyte was 0.1 M $(C_4H_9)_4NClO_4$ in acetonitrile. Reproduced with permission from ref. 266 Copyright 2011, Elsevier. (h) Chemical structures of ferrocene-functionalized polyheteroacenes, namely **P1** and **P2**. (i) Cycling performances of **P1** and **P2** ferrocene-functionalized polyheteroacenes under 0.1C. Reproduced with permission from ref. 239 Copyright 2018, The Royal Society of Chemistry.

capacity retention over multiple cycles, showcasing their suitability for battery applications (Fig. 12i). Together, these studies highlight the potential of organic–inorganic hybrid materials as electrodes for high-performance LIBs.

4.3 Copolymer materials

Recently, copolymerization has emerged as an alternative approach to enhance the electrochemical performance of polymer-based electrodes. These materials typically consist of two or more different polymerized monomer units, offering synergistic benefits compared to individual polymers.[270,271] One notable advantage of copolymer materials is their ability to combine the desirable properties of different polymer components. For example, copolymers can incorporate both electron-rich and electron-deficient monomers, enabling improved charge transfer kinetics and stability during cycling. Additionally, the incorporation of various functional groups within copolymer structures can be introduced to facilitate rapid lithium-ion diffusion and enhance the number of active sites.[271] Moreover, copolymer materials often offer enhanced mechanical strength and flexibility compared to individual polymer or traditional inorganic electrodes, making them suitable for use in flexible and lightweight battery applications.[272] Furthermore, copolymer-based electrodes can be processed using scalable

solution-based techniques, enabling cost-effective and large-scale manufacturing.

Recent research efforts have focused on designing copolymer materials with tailored properties for specific battery applications. For instance, copolymers containing conjugated backbones, such as polythiophenes and polypyrrole, have been investigated due to their high electrical conductivity and lithium-ion storage capacity.[92,273] Additionally, copolymers incorporating redox-active moieties, such as viologen and anthraquinone, have shown promise for achieving high capacity and long-term cycling stability.[274] Copolymers such as that derived from pyrrole and dopamine (**PPy-DA**) offer distinct advantages in LIB applications by combining the charge storage properties of different monomers.[275] The copolymer presented a porous NF morphology, which was different from the plate-like structure of **PDA** and the aggregated nanospheres of **PPy** (Fig. 13a–c). **PPy-DA** was produced *via* the copolymerization of dopamine (n-type) and **PPy** (p-type) monomer, leading to a copolymer with a shorter polaron delocalization length. This reduction in delocalization was effective in enhancing its redox potential (around 3–3.5 V) and specific capacity (~160 mA h g⁻¹) (Fig. 13d). Furthermore, two novel copolymers, namely poly(-dihydrophenazine-*co*-diphenylamine) (**PDPAPZ**) and poly(-dihydrophenazine-*co*-phenothiazine) (**PPTZPZ**), were synthesized and evaluated as cathode materials (Fig. 13e and f),
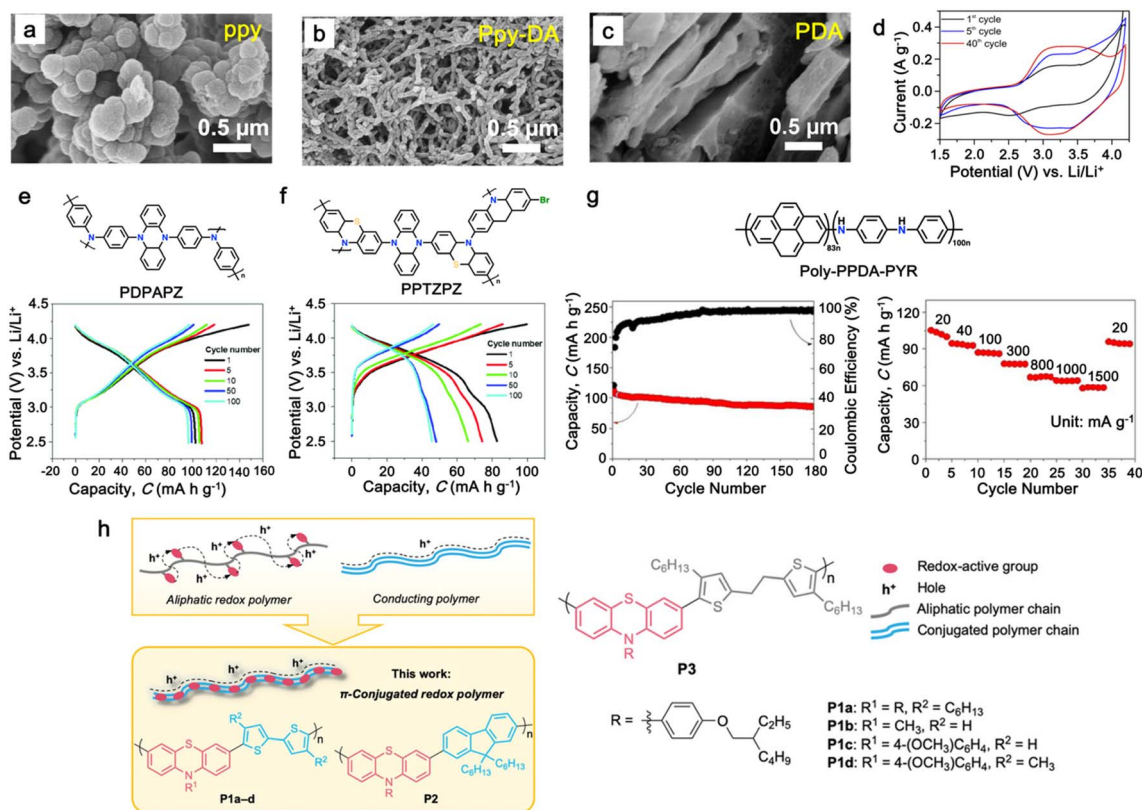
This journal is © The Royal Society of Chemistry 2025

J. Mater. Chem. A, 2025, **13**, 1552–1589 | **1581**

Fig. 13 SEM images of (a) **PPy**, (b) **PPy-DA**, and (c) **PDA**. (d) CV curves of **PPy-DA** at a scan rate of 1 mV s^{-1}. Reproduced with permission from ref. 275 Copyright 2018, Elsevier. (e) and (f) Chemical structure and galvanostatic charge–discharge of **PDPAPZ** and **PPTZPZ** copolymers, respectively. Reproduced with permission from ref. 179 Copyright 2020, John Wiley and Sons. (g) Cycling performance at a current density of 20 mA g^{-1} and rate performance of **poly-PPDA-PYR** copolymer. Reproduced with permission from ref. 246 Copyright 2019, John Wiley and Sons. (h) Schematic of the π-conjugated redox polymer. Reproduced with permission from ref. 276 Copyright 2019, John Wiley and Sons.

respectively.[179] These copolymers exhibited a high average discharge potential (3.5–3.6 V) in lithium cells. Remarkably, the **PDPAPZ**/Li cells demonstrated a steady specific capacity of ~101 mA h g^{-1} at a current density of 0.1 A g^{-1} up to 100 cycles (Fig. 13e). Alternatively, **PPTZPZ** exhibited a lower capacity of 80 mA h g^{-1} and later demonstrated a gradual decrease in capacity up to 100 cycles (Fig. 13f) due to the inactive sulfur species. Similarly, Yao and colleagues synthesized a new conjugated copolymer for use as an organic cathode material by incorporating both conducting aniline and pyrene units (Fig. 13g).[246] This **poly-PPDA-PYR** achieved a reversible specific capacity of 113 mA h g^{-1} at a current density of 20 mA g^{-1} with a high voltage output of 3.2 V and impressive capacity retention of 75.2% after 180 cycles (Fig. 13g). Additionally, the copolymer exhibited an excellent rate performance of up to 1500 mA g^{-1}, and the highest specific capacity ~100 mA h g^{-1} could be recovered once the current density switched back to 20 mA g^{-1} (Fig. 13g).

In addition to the copolymerization of redox-active components, the incorporation of inactive components into copolymers has also been extensively investigated due to their impact on the electrochemical performance. These inactive components serve various functions such as enhancing the cycle stability, electrical conductivity, ionic conductivity, cohesiveness, and flexibility;

however, a reduced theoretical capacity is often observed.[276] For instance, Hernández et al. combined a redox-active polyimide (**PI**) with ion-conductive polyether blocks (**PEO**), where **PEO** acted as both a binder and conductive agent.[244] The resulting binder-free and conductive agent-free copolymer electrode exhibited an excellent discharge capacity and cycling life. Similarly, Zhang et al. synthesized a copolymer based on poly(2,2,6,6-tetramethylpiperidinyloxy methacrylate) (**PTMA**) with controllable pyrene side groups, which enhanced the electron transfer rates and resulted in improved specific capacity and rate capability when uniformly dispersed in a composite with reduced graphene oxide (**rGO**).[219] Additionally, an ultra-high-rate capability and long stability were demonstrated using phenothiazine copolymer.[276] The design of this copolymer cathode was based on the combination of the high oxidation of phenothiazine at 3.6 V (vs. Li/Li$^+$) and good hole conductivity of the bithiophene and fluorene comonomer (Fig. 13h). An ultra-high-rate capability and long cycling stability were demonstrated given that the π-conjugated copolymer could be operated for up to 30 000 cycles at an extreme current rate of 100C with >97% capacity retention. These studies emphasized the importance of the copolymerization strategy to enhance the electrochemical performance of the polymer cathode.

1582 | J. Mater. Chem. A, 2025, **13**, 1552–1589

This journal is © The Royal Society of Chemistry 2025

5. Conclusions and perspective

Polymeric electrode materials have emerged as promising alternative cathode materials towards high-performance and high-energy-density 4.0 V-class organic LIBs. By tailoring their chemical structure through functionalization, doping, and incorporating both redox-active and inactive components, researchers can optimize the key parameters of batteries such as specific capacity, cycling stability, and rate capability. This innovative approach addresses many of the limitations associated with traditional electrode materials, paving the way for more efficient, durable, and high-performing LIBs. As the demand for higher energy storage solutions continues to grow, the advancements in polymeric electrode design are poised to play a crucial role in meeting the energy needs of the future. Owing to their flexibility in design, scalability of synthesis, and compatibility with high-energy-density applications compared to the conventional inorganic cathode materials, a series of high-voltage polymers such as arylamine-based, thioether, phenazine, viologen and radical polymers has been explored and discussed in detail. Additionally, alternative approaches such as the formation of bipolar polymers and hybrid organic–inorganic polymers and copolymerization strategies have also been shown to be promising to enhance the electrochemical performance and stability of polymer cathodes. By harnessing the unique properties of each polymer, such as tunable redox chemistry, mechanical flexibility, and chemical stability, researchers have unlocked new possibilities for achieving a superior electrochemical performance in LIBs. Moving forward, continued research efforts in this field will be essential to further optimize the design and synthesis of polymeric-based electrode materials, paving the way for the next generation of high-performance LIBs.

Looking ahead, the future of polymeric electrode materials for high-energy-density LIBs holds exciting prospects and challenges. Firstly, it is necessary to gain a deeper understanding of the fundamental electrochemical processes occurring within polymer electrodes, including the ion transport mechanisms, charge storage mechanisms, and degradation pathways. In this case, advanced characterization techniques, coupled with computational modeling, will play a crucial role in elucidating these complex phenomena and guiding the rational design of next-generation polymer electrodes. Furthermore, efforts should be directed towards the development of scalable synthesis methods for producing polymer materials with well-defined structures and tailored properties. The integration of advanced manufacturing techniques, such as additive manufacturing and roll-to-roll processing, will enable the fabrication of large-area, high-performance polymer electrodes for practical applications. Additionally, research should focus on exploring novel polymer chemistries, functionalization strategies, and electrode architectures to further enhance the energy density, safety, and lifespan of 4.0 V-class organic LIBs. Additionally, collaboration among academia, industry, and government institutions will be crucial for accelerating the translation of research findings into commercial products.

Investment in infrastructure, pilot-scale production facilities, and collaborative research initiatives will facilitate the transition of polymeric electrode materials from the laboratory to the marketplace. Ultimately, the continued advancement of polymeric electrode materials holds immense potential to drive innovation in energy storage technology and address the growing demand for high-performance LIBs in a wide range of applications.

Data availability

The data supporting this article have been included as Notes and references.

Author contributions

Conceptualization and methodology: F. B. and H. J. Y. Investigation: F. B., S. U. S. and A. L. L. Writing-original draft: F. B. and S. U. S. Writing – review & editing: F. B., S. U. S., and H. J. Y. Visualization: F. B. Supervision: H. J. Y. All authors discussed the results and reviewed the manuscript.

Conflicts of interest

There are no conflicts to declare.

Acknowledgements

Notes and references

1 Y. Ding, Z. P. Cano, A. Yu, J. Lu and Z. Chen, *Electrochem. Energy Rev.*, 2019, **2**, 1–28.

2 J. Xie and Y.-C. Lu, *Nat. Commun.*, 2020, **11**, 2499.

3 C. N. Gannett, L. Melecio-Zambrano, M. J. Theibault, B. M. Peterson, B. P. Fors and H. D. Abruña, *Mater. Rep.: Energy*, 2021, **1**, 100008.

4 T. Wulandari, D. Fawcett, S. B. Majumder and G. E. J. Poinern, *Battery Energy*, 2023, **2**, 20230030.

5 C. P. Grey and D. S. Hall, *Nat. Commun.*, 2020, **11**, 6279.

6 A. Manthiram, *Nat. Commun.*, 2020, **11**, 1550.

7 B. Dunn, H. Kamath and J.-M. Tarascon, *Science*, 2011, **334**, 928–935.

8 J. B. Goodenough and K.-S. Park, *J. Am. Chem. Soc.*, 2013, **135**, 1167–1176.

9 C. Liu, Z. G. Neale and G. Cao, *Mater. Today*, 2016, **19**, 109–123.

10 A. Saxena, N. Gnanaseelan, S. K. Kamaraj and F. Caballero-Briones, in *Rechargeable Lithium-Ion Batteries*, CRC Press, 2020, pp. 260–288.

11 J. M. Tarascon and M. Armand, *Nature*, 2001, **414**, 359–367.

This journal is © The Royal Society of Chemistry 2025

J. Mater. Chem. A, 2025, **13**, 1552–1589 | **1583**

12 J. Li, C. Lin, M. Weng, Y. Qiu, P. Chen, K. Yang, W. Huang, Y. Hong, J. Li, M. Zhang, C. Dong, W. Zhao, Z. Xu, X. Wang, K. Xu, J. Sun and F. Pan, *Nat. Nanotechnol.*, 2021, **16**, 599–605.

13 B. Tao, I. J. McPherson, E. Daviddi, C. L. Bentley and P. R. Unwin, *ACS Sustainable Chem. Eng.*, 2023, **11**, 1459–1471.

14 D. D. MacNeil, Z. Lu and J. R. Dahn, *J. Electrochem. Soc.*, 2002, **149**, A1332.

15 M. V. Reddy, G. V. Subba Rao and B. V. R. Chowdari, *Chem. Rev.*, 2013, **113**, 5364–5457.

16 F. Wu, J. Maier and Y. Yu, *Chem. Soc. Rev.*, 2020, **49**, 1569–1614.

17 S. Gantenbein, M. Schönleber, M. Weiss and E. Ivers-Tiffée, *Sustainability*, 2019, **11**(23), 6697.

18 C. Zeng, F. Fan, R. Zheng, X. Wang, G. Tian, S. Liu, P. Liu, C. Wang, S. Wang and C. Shu, *ACS Appl. Mater. Interfaces*, 2024, **16**, 11377–11388.

19 B. Xu, D. Qian, Z. Wang and Y. S. Meng, *Mater. Sci. Eng., R*, 2012, **73**, 51–65.

20 S. Zhao, K. Yan, J. Zhang, B. Sun and G. Wang, *Angew. Chem., Int. Ed.*, 2021, **60**, 2208–2220.

21 K. Amin, L. Mao and Z. Wei, *Macromol. Rapid Commun.*, 2019, **40**, 1800565.

22 Z. Song and H. Zhou, *Energy Environ. Sci.*, 2013, **6**, 2280–2301.

23 H. Ji, J. Wu, Z. Cai, J. Liu, D.-H. Kwon, H. Kim, A. Urban, J. K. Papp, E. Foley, Y. Tian, M. Balasubramanian, H. Kim, R. J. Clément, B. D. McCloskey, W. Yang and G. Ceder, *Nat. Energy*, 2020, **5**, 213–221.

24 M. Malik, K. H. Chan and G. Azimi, *Mater. Today Energy*, 2022, **28**, 101066.

25 K. Liu, Y. Liu, D. Lin, A. Pei and Y. Cui, *Sci. Adv.*, 2018, **4**, eaas9820.

26 B. Häupler, A. Wild and U. S. Schubert, *Adv. Energy Mater.*, 2015, **5**, 1402034.

27 P. Poizot, J. Gaubicher, S. Renault, L. Dubois, Y. Liang and Y. Yao, *Chem. Rev.*, 2020, **120**, 6490–6557.

28 W. Du, X. Du, M. Ma, S. Huang, X. Sun and L. Xiong, *Adv. Funct. Mater.*, 2022, **32**, 2110871.

29 S. Lee, J. E. Kwon, J. Hong, S. Y. Park and K. Kang, *J. Mater. Chem. A*, 2019, **7**, 11438–11443.

30 A. Wild, M. Strumpf, B. Häupler, M. D. Hager and U. S. Schubert, *Adv. Energy Mater.*, 2017, **7**, 1601415.

31 L. M. Zhu, A. W. Lei, Y. L. Cao, X. P. Ai and H. X. Yang, *Chem. Commun.*, 2013, **49**, 567–569.

32 K. Hatakeyama-Sato, T. Tezuka, R. Ichinoi, S. Matsumono, K. Sadakuni and K. Oyaizu, *ChemSusChem*, 2020, **13**, 2443–2448.

33 É. Deunf, P. Moreau, É. Quarez, D. Guyomard, F. Dolhem and P. Poizot, *J. Mater. Chem. A*, 2016, **4**, 6131–6139.

34 D. Larcher and J.-M. Tarascon, *Nat. Chem.*, 2015, **7**, 19–29.

35 M. E. Baumert, V. Le, P.-H. Su, Y. Akae, D. Bresser, P. Théato and M. M. Hansmann, *J. Am. Chem. Soc.*, 2023, **145**, 23334–23345.

36 H. Kye, Y. Kang, D. Jang, J. E. Kwon and B.-G. Kim, *Adv. Energy Sustainability Res.*, 2022, **3**, 2200030.

37 D. J. Min, K. Lee, S. Y. Park and J. E. Kwon, *ChemSusChem*, 2020, **13**, 2303–2311.

38 X. Liu and Z. Ye, *Adv. Energy Mater.*, 2021, **11**, 2003281.

39 Y. Hu, Y. Gao, L. Fan, Y. Zhang, B. Wang, Z. Qin, J. Zhou and B. Lu, *Adv. Energy Mater.*, 2020, **10**, 2002780.

40 F. Cheng, J. Liang, Z. Tao and J. Chen, *Adv. Mater.*, 2011, **23**, 1695–1715.

41 S. Lee, G. Kwon, K. Ku, K. Yoon, S. K. Jung, H. D. Lim and K. Kang, *Adv. Mater.*, 2018, **30**, 1704682.

42 X. Feng, X. Chen, B. Ren, X. Wu, X. Huang, R. Ding, X. Sun, S. Tan, E. Liu and P. Gao, *ACS Appl. Mater. Interfaces*, 2021, **13**, 7178–7187.

43 R. Chen, D. Bresser, M. Saraf, P. Gerlach, A. Balducci, S. Kunz, D. Schröder, S. Passerini and J. Chen, *ChemSusChem*, 2020, **13**, 2205–2219.

44 J. Heiska, M. Nisula and M. Karppinen, *J. Mater. Chem. A*, 2019, **7**, 18735–18758.

45 Z. Song, H. Zhan and Y. Zhou, *Angew. Chem., Int. Ed.*, 2010, **49**, 8444–8448.

46 T. Nokami, T. Matsuo, Y. Inatomi, N. Hojo, T. Tsukagoshi, H. Yoshizawa, A. Shimizu, H. Kuramoto, K. Komae and H. Tsuyama, *J. Am. Chem. Soc.*, 2012, **134**, 19694–19700.

47 S. Muench, A. Wild, C. Friebe, B. Haupler, T. Janoschka and U. S. Schubert, *Chem. Rev.*, 2016, **116**, 9438–9484.

48 J. Yang, Z. Wang, Y. Shi, P. Sun and Y. Xu, *ACS Appl. Mater. Interfaces*, 2020, **12**, 7179–7185.

49 T. Cai, Y. Han, Q. Lan, F. Wang, J. Chu, H. Zhan and Z. Song, *Energy Storage Mater.*, 2020, **31**, 318–327.

50 F. Wan, X.-L. Wu, J.-Z. Guo, J.-Y. Li, J.-P. Zhang, L. Niu and R.-S. Wang, *Nano Energy*, 2015, **13**, 450–457.

51 Y. Wang, Y. Ding, L. Pan, Y. Shi, Z. Yue, Y. Shi and G. Yu, *Nano Lett.*, 2016, **16**, 3329–3334.

52 M. Lee, J. Hong, J. Lopez, Y. Sun, D. Feng, K. Lim, W. C. Chueh, M. F. Toney, Y. Cui and Z. Bao, *Nat. Energy*, 2017, **2**, 861–868.

53 Q. Dong, T. Naren, L. Zhang, W. Jiang, M. Xue, X. Wang, L. Chen, C.-S. Lee and Q. Zhang, *Angew. Chem., Int. Ed.*, 2024, **63**, e202405426.

54 W. Guo, Y.-X. Yin, S. Xin, Y.-G. Guo and L.-J. Wan, *Energy Environ. Sci.*, 2012, **5**, 5221–5225.

55 Z. Song, T. Xu, M. L. Gordin, Y.-B. Jiang, I.-T. Bae, Q. Xiao, H. Zhan, J. Liu and D. Wang, *Nano Lett.*, 2012, **12**, 2205–2211.

56 C. Luo, Y. Zhu, Y. Xu, Y. Liu, T. Gao, J. Wang and C. Wang, *J. Power Sources*, 2014, **250**, 372–378.

57 C. Peng, G.-H. Ning, J. Su, G. Zhong, W. Tang, B. Tian, C. Su, D. Yu, L. Zu, J. Yang, M.-F. Ng, Y.-S. Hu, Y. Yang, M. Armand and K. P. Loh, *Nat. Energy*, 2017, **2**, 17074.

58 K. B. Labasan, H.-J. Lin, F. Baskoro, J. J. H. Togonon, H. Q. Wong, C.-W. Chang, S. D. Arco and H.-J. Yen, *ACS Appl. Mater. Interfaces*, 2021, **13**, 17467–17477.

59 J. Wang, H. Liu, C. Du, X. Zhang, Y. Liu, H. Yao, Z. Sun and S. Guan, *Chem. Eng. J.*, 2022, **444**, 136598.

60 X.-Y. Han, C.-X. Chang, L.-J. Yuan, T.-L. Sun and J. Sun, *Adv. Mater.*, 2007, **19**, 1616–1621.

61 J. Kim, J. H. Kim and K. Ariga, *Joule*, 2017, **1**, 739–768.

1584 | *J. Mater. Chem. A*, 2025, **13**, 1552–1589

This journal is © The Royal Society of Chemistry 2025

62 F. Baskoro, A. L. Lubis, H. Q. Wong, G.-S. Liou and H.-J. Yen, *J. Mater. Chem. A*, 2023, **11**, 11210–11221.

63 F. Baskoro, H.-J. Lin, C.-W. Chang, C.-L. Wang, A. L. Lubis and H.-J. Yen, *J. Mater. Chem. A*, 2023, **11**, 569–578.

64 A. L. Lubis, F. Baskoro, T.-H. Lin, H. Q. Wong, G.-S. Liou and H.-J. Yen, *ACS Appl. Mater. Interfaces*, 2024, **16**, 48722–48735.

65 J. Sun, Y. Xu, Y. Lv, Q. Zhang and X. Zhou, *CCS Chem.*, 2023, **5**, 1259–1276.

66 M. Majumder, A. K. Thakur, A. S. Patole and S. P. Patole, in *Organic Electrodes: Fundamental to Advanced Emerging Applications*, ed. R. K. Gupta, Springer International Publishing, Cham, 2022, pp. 171–188.

67 Z. Yang, F. Wang, P. Meng, J. Luo and C. Fu, *Energy Storage Mater.*, 2022, **51**, 63–79.

68 F. Goto, K. Abe, K. Ikabayashi, T. Yoshida and H. Morimoto, *J. Power Sources*, 1987, **20**, 243–248.

69 M. Kobayashi, N. Colaneri, M. Boysel, F. Wudl and A. J. Heeger, *J. Chem. Phys.*, 1985, **82**, 5717–5723.

70 S. Taguchi and T. Tanaka, *J. Power Sources*, 1987, **20**, 249–252.

71 L. W. Shacklette, R. L. Elsenbaumer, R. R. Chance, J. M. Sowa, D. M. Ivory, G. G. Miller and R. H. Baughman, *J. Chem. Soc., Chem. Commun.*, 1982, 361–362.

72 K. Nakahara, S. Iwasa, M. Satoh, Y. Morioka, J. Iriyama, M. Suguro and E. Hasegawa, *Chem. Phys. Lett.*, 2002, **359**, 351–354.

73 W. Choi, D. Harada, K. Oyaizu and H. Nishide, *J. Am. Chem. Soc.*, 2011, **133**, 19839–19843.

74 T. Suga, M. Sakata, K. Aoki and H. Nishide, *ACS Macro Lett.*, 2014, **3**, 703–707.

75 Z. Song, Y. Qian, M. L. Gordin, D. Tang, T. Xu, M. Otani, H. Zhan, H. Zhou and D. Wang, *Angew. Chem.*, 2015, **127**, 14153–14157.

76 K. Zhang, C. Guo, Q. Zhao, Z. Niu and J. Chen, *Adv. Sci.*, 2015, **2**, 1500018.

77 J. E. Kwon, C.-S. Hyun, Y. J. Ryu, J. Lee, D. J. Min, M. J. Park, B.-K. An and S. Y. Park, *J. Mater. Chem. A*, 2018, **6**, 3134–3140.

78 W. Huang, Z. Zhu, L. Wang, S. Wang, H. Li, Z. Tao, J. Shi, L. Guan and J. Chen, *Angew. Chem., Int. Ed.*, 2013, **52**, 9162–9166.

79 H. Senoh, M. Yao, H. Sakaebe, K. Yasuda and Z. Siroma, *Electrochim. Acta*, 2011, **56**, 10145–10150.

80 Y. Liang, P. Zhang, S. Yang, Z. Tao and J. Chen, *Adv. Energy Mater.*, 2013, **3**, 600–605.

81 Q. Zhao, J. Wang, C. Chen, T. Ma and J. Chen, *Nano Res.*, 2017, **10**, 4245–4255.

82 Y. Shi, H. Tang, S. Jiang, L. V. Kayser, M. Li, F. Liu, F. Ji, D. J. Lipomi, S. P. Ong and Z. Chen, *Chem. Mater.*, 2018, **30**, 3508–3517.

83 M. Lee, J. Hong, B. Lee, K. Ku, S. Lee, C. B. Park and K. Kang, *Green Chem.*, 2017, **19**, 2980–2985.

84 G. Dai, X. Wang, Y. Qian, Z. Niu, X. Zhu, J. Ye, Y. Zhao and X. Zhang, *Energy Storage Mater.*, 2019, **16**, 236–242.

85 J. Kim, H.-S. Park, T.-H. Kim, S. Y. Kim and H.-K. Song, *Phys. Chem. Chem. Phys.*, 2014, **16**, 5295–5300.

86 M. Yao, H. Senoh, T. Sakai and T. Kiyobayashi, *J. Power Sources*, 2012, **202**, 364–368.

87 C. Zhang, X. Yang, W. Ren, Y. Wang, F. Su and J.-X. Jiang, *J. Power Sources*, 2016, **317**, 49–56.

88 C. Su, F. Yang, L. Ji, L. Xu and C. Zhang, *J. Mater. Chem. A*, 2014, **2**, 20083–20088.

89 K. Lee, I. E. Serdiuk, G. Kwon, D. J. Min, K. Kang, S. Y. Park and J. E. Kwon, *Energy Environ. Sci.*, 2020, **13**, 4142–4156.

90 M. Li, R. Wang, T. Wu, Y. Liu, Y. Chen, W. He, S. Feng, X. Zhang, G. Dai and Y. Zhao, *ACS Appl. Energy Mater.*, 2023, **6**, 6834–6841.

91 H. Park, H. Kye, J.-S. Lee, Y.-C. Joo, D. J. Min, B.-G. Kim, S. Y. Park and J. E. Kwon, *Energy Environ. Mater.*, 2024, **7**, e12694.

92 S. Lee, G. Kwon, T. Kang, J. Kim, B. Lee, C. Kim, C. Lee, Y. Kim, J. Noh, Y.-S. Yu, D. Lee and K. Kang, *J. Mater. Chem.*, 2023, **11**, 22441–22448.

93 M. S. Whittingham, *Chem. Rev.*, 2004, **104**, 4271–4302.

94 J. Xu, X. Cai, S. Cai, Y. Shao, C. Hu, S. Lu and S. Ding, *Energy Environ. Mater.*, 2023, **6**, e12450.

95 M. S. Whittingham, *Chem. Rev.*, 2014, **114**, 11414–11443.

96 S. V. Venkatesan, A. Nandy, K. Karan, S. R. Larter and V. Thangadurai, *Electrochem. Energy Rev.*, 2022, **5**, 16.

97 R. Hildner, A. Köhler, P. Müller-Buschbaum, F. Panzer and M. Thelakkat, *Adv. Energy Mater.*, 2017, **7**, 1700314.

98 S. Wang, G. Zuo, J. Kim and H. Sirringhaus, *Prog. Polym. Sci.*, 2022, **129**, 101548.

99 H. Sun, F. Chen and Z.-K. Chen, *Mater. Today*, 2019, **24**, 94–118.

100 J.-H. Dou, Z.-A. Yu, J. Zhang, Y.-Q. Zheng, Z.-F. Yao, Z. Tu, X. Wang, S. Huang, C. Liu, J. Sun, Y. Yi, X. Cao, Y. Gao, J.-Y. Wang and J. Pei, *J. Am. Chem. Soc.*, 2019, **141**, 6561–6568.

101 C. Bian, S. Wang, Y. Liu and X. Jing, *RSC Adv.*, 2016, **6**, 55007–55016.

102 A. Onwubiko, W. Yue, C. Jellett, M. Xiao, H.-Y. Chen, M. K. Ravva, D. A. Hanifi, A.-C. Knall, B. Purushothaman, M. Nikolka, J.-C. Flores, A. Salleo, J.-L. Bredas, H. Sirringhaus, P. Hayoz and I. McCulloch, *Nat. Commun.*, 2018, **9**, 416.

103 H. Usta, C. Risko, Z. Wang, H. Huang, M. K. Deliomeroglu, A. Zhukhovitskiy, A. Facchetti and T. J. Marks, *J. Am. Chem. Soc.*, 2009, **131**, 5586–5608.

104 S. Fratini, M. Nikolka, A. Salleo, G. Schweicher and H. Sirringhaus, *Nat. Mater.*, 2020, **19**, 491–502.

105 S. Prodhan, J. Qiu, M. Ricci, O. M. Roscioni, L. Wang and D. Beljonne, *J. Phys. Chem. Lett.*, 2020, **11**, 6519–6525.

106 K. H. Hendriks, W. Li, M. M. Wienk and R. A. J. Janssen, *J. Am. Chem. Soc.*, 2014, **136**, 12130–12136.

107 H. Bronstein, C. B. Nielsen, B. C. Schroeder and I. McCulloch, *Nat. Rev. Chem.*, 2020, **4**, 66–77.

108 S. Bitton and N. Tessler, *Adv. Electron. Mater.*, 2024, 2300766.

109 K. D. Fong, J. Self, K. M. Diederichsen, B. M. Wood, B. D. McCloskey and K. A. Persson, *ACS Cent. Sci.*, 2019, **5**, 1250–1260.

This journal is © The Royal Society of Chemistry 2025

J. Mater. Chem. A, 2025, **13**, 1552–1589 | **1585**

110 T. Junkers, J. Vandenbergh, P. Adriaensens, L. Lutsen and D. Vanderzande, *Polym. Chem.*, 2012, **3**, 275–285.

111 A. Chamas, H. Moon, J. Zheng, Y. Qiu, T. Tabassum, J. H. Jang, M. Abu-Omar, S. L. Scott and S. Suh, *ACS Sustainable Chem. Eng.*, 2020, **8**, 3494–3511.

112 T. L. D. Tam, M. Lin, S. W. Chien and J. Xu, *ACS Macro Lett.*, 2021, **11**, 110–115.

113 A. Dai, A. Wan, C. Magee, Y. Zhang, S. Barlow, S. R. Marder and A. Kahn, *Org. Electron.*, 2015, **23**, 151–157.

114 I. M. Ward and J. Sweeney, *Mechanical Properties of Solid Polymers*, John Wiley & Sons, 2012.

115 H.-Y. Wu, J.-D. Huang, S. Y. Jeong, T. Liu, Z. Wu, T. van der Pol, Q. Wang, M.-A. Stoeckel, Q. Li and M. Fahlman, *Mater. Horiz.*, 2023, **10**, 4213–4223.

116 L. Bondi, C. Marzuoli, E. Gutiérrez-Fernández, G. Tullii, J. Martín, B. Fraboni, D. Mecerreyes, M. R. Antognazza and T. Cramer, *Adv. Electron. Mater.*, 2023, **9**, 2300146.

117 I. K. Yakushchenko, M. G. Kaplunov, O. N. Efimov, M. Y. Belov and S. N. Shamaev, *Phys. Chem. Chem. Phys.*, 1999, **1**, 1783–1785.

118 C. Zhang, S. Chen, G. Zhou, Q. Hou, S. Luo, Y. Wang and G. Shi, *J. Electrochem. Soc.*, 2021, **168**, 050548.

119 C. Su, H. He, L. Xu, K. Zhao, C. Zheng and C. Zhang, *J. Mater. Chem. A*, 2017, **5**, 2701–2709.

120 J. K. Feng, Y. L. Cao, X. P. Ai and H. X. Yang, *J. Power Sources*, 2008, **177**, 199–204.

121 Z. Chen, C. Su, X. Zhu, R. Xu, L. Xu and C. Zhang, *J. Polym. Sci., Part A: Polym. Chem.*, 2018, **56**, 2574–2583.

122 K. Yamamoto, D. Suemasa, K. Masuda, K. Aita and T. Endo, *ACS Appl. Mater. Interfaces*, 2018, **10**, 6346–6353.

123 Z. Chen, W. Li, Y. Dai, N. Xu, C. Su, J. Liu and C. Zhang, *Electrochim. Acta*, 2018, **286**, 187–194.

124 Y. Ou, Y. Xiong, Z. Hu, Y. Zhang and L. Dong, *J. Mater. Chem. A*, 2022, **10**, 10373–10382.

125 F. A. Obrezkov, A. F. Shestakov, S. G. Vasil'ev, K. J. Stevenson and P. A. Troshin, *J. Mater. Chem. A*, 2021, **9**, 2864–2871.

126 I. Kang, T. Lee, Y. R. Yoon, J. W. Kim, B.-K. Kim, J. Lee, J. H. Lee and S. Y. Kim, *Mater*, 2021, **14**, 7885.

127 W. Huang, T. Jia, G. Zhou, S. Chen, Q. Hou, Y. Wang, S. Luo, G. Shi and B. Xu, *Electrochim. Acta*, 2018, **283**, 1284–1290.

128 C. Su, X. Zhu, L. Xu, N. Zhou, H. He and C. Zhang, *Electrochim. Acta*, 2016, **196**, 440–449.

129 L. Zhu and X. Cao, *Mater. Lett.*, 2015, **150**, 16–19.

130 C. Su, L. Ji, L. Xu, N. Zhou, G. Wang and C. Zhang, *RSC Adv.*, 2016, **6**, 22989–22995.

131 J. Xiong, Z. Wei, T. Xu, Y. Zhang, C. Xiong and L. Dong, *Polymer*, 2017, **130**, 135–142.

132 T. Xu, J. Xiong, X. Du, Y. Zhang, S. Song, C. Xiong and L. Dong, *J. Phys. Chem. C*, 2018, **122**, 20057–20063.

133 X. Zhao, C. Wang, Z. Li, X. Hu, A. A. Razzaq and Z. Deng, *J. Mater. Chem. A*, 2021, **9**, 19282–19297.

134 Y. Liang, Z. Tao and J. Chen, *Adv. Energy Mater.*, 2012, **2**, 742–769.

135 P. Sang, Q. Chen, D.-Y. Wang, W. Guo and Y. Fu, *Chem. Rev.*, 2023, **123**, 1262–1326.

136 X. Zhang, W. Guo and Y. Fu, *Acc. Mater. Res.*, 2024, **5**, 316–328.

137 M. A. Weret, C.-F. J. Kuo, W.-N. Su, T. S. Zeleke, C.-J. Huang, N. A. Sahalie, T. A. Zegeye, Z. T. Wondimkun, F. W. Fenta, B. A. Jote, M.-C. Tsai and B. J. Hwang, *J. Power Sources*, 2022, **541**, 231693.

138 Y. Chen, S. Zhuo, Z. Li and C. Wang, *EnergyChem*, 2020, **2**, 100030.

139 D.-Y. Wang, W. Guo and Y. Fu, *Acc. Chem. Res.*, 2019, **52**, 2290–2300.

140 W. Guo, D. Y. Wang, Q. Chen and Y. Fu, *Adv. Sci.*, 2022, **9**, 2103989.

141 M. J. H. Worthington, R. L. Kucera and J. M. Chalker, *Green Chem.*, 2017, **19**, 2748–2761.

142 J. Ren, X. Wang, H. Liu, Y. Hu, X. Zhang and T. Masuda, *React. Funct. Polym.*, 2020, **146**, 104365.

143 D. Ogi, Y. Fujita, M. Kato, T. Yamauchi, T. Shirahata, M. Yao and Y. Misaki, *Eur. J. Org Chem.*, 2019, **2019**, 2725–2728.

144 J. Ren, X. Wang, H. Liu, Y. Hu, X. Zhang and T. Masuda, *React. Funct. Polym.*, 2020, **146**, 104365.

145 T. P. Vaid, M. E. Easton and R. D. Rogers, *Synth. Met.*, 2017, **231**, 44–50.

146 D. Ogi, Y. Fujita, M. Kato, T. Yamauchi, T. Shirahata, M. Yao and Y. Misaki, *Eur. J. Org Chem.*, 2019, **2019**, 2725–2728.

147 J. Tang, L. Kong, J. Zhang, L. Zhan, H. Zhan, Y. Zhou and C. Zhan, *React. Funct. Polym.*, 2008, **68**, 1408–1413.

148 L. Zhan, Z. Song, N. Shan, J. Zhang, J. Tang, H. Zhan, Y. Zhou, Z. Li and C. Zhan, *J. Power Sources*, 2009, **193**, 859–863.

149 M. E. Speer, M. Kolek, J. J. Jassoy, J. Heine, M. Winter, P. M. Bieker and B. Esser, *Chem. Commun.*, 2015, **51**, 15261–15264.

150 B. Häupler, R. Burges, C. Friebe, T. Janoschka, D. Schmidt, A. Wild and U. S. Schubert, *Macromol. Rapid Commun.*, 2014, **35**, 1367–1371.

151 P. Sang, Y. Si and Y. Fu, *Chem. Commun.*, 2019, **55**, 4857–4860.

152 M. B. Preefer, B. Oschmann, C. J. Hawker, R. Seshadri and F. Wudl, *Angew. Chem., Int. Ed.*, 2017, **56**, 15118–15122.

153 Y. Jing, Y. Liang, S. Gheytani and Y. Yao, *Nano Energy*, 2017, **37**, 46–52.

154 B. Häupler, T. Hagemann, C. Friebe, A. Wild and U. S. Schubert, *ACS Appl. Mater. Interfaces*, 2015, **7**, 3473–3479.

155 A. Bhargav, M. E. Bell, Y. Cui and Y. Fu, *ACS Appl. Energy Mater.*, 2018, **1**, 5859–5864.

156 P. Sang, J. Song, W. Guo and Y. Fu, *Chem. Eng. J.*, 2021, **415**, 129043.

157 A. Bhargav, C.-H. Chang, Y. Fu and A. Manthiram, *ACS Appl. Mater. Interfaces*, 2019, **11**, 6136–6142.

158 S. H. Je, T. H. Hwang, S. N. Talapaneni, O. Buyukcakir, H. J. Kim, J.-S. Yu, S.-G. Woo, M. C. Jang, B. K. Son, A. Coskun and J. W. Choi, *ACS Energy Lett.*, 2016, **1**, 566–572.

1586 | *J. Mater. Chem. A*, 2025, **13**, 1552–1589

This journal is © The Royal Society of Chemistry 2025

159 H. Kim, J. Lee, H. Ahn, O. Kim and M. J. Park, *Nat. Commun.*, 2015, **6**, 7278.

160 S. Zeng, L. Li, D. Zhao, J. Liu, W. Niu, N. Wang and S. Chen, *J. Phys. Chem. C*, 2017, **121**, 2495–2503.

161 R. F. Nelson, D. W. Leedy, E. T. Seo and R. N. Adams, *Fresenius' Z. Anal. Chem.*, 1966, **224**, 184–196.

162 Z. Niu, H. Wu, L. Liu, G. Dai, S. Xiong, Y. Zhao and X. Zhang, *J. Mater. Chem. A*, 2019, **7**, 10581–10588.

163 C. N. Gannett, B. M. Peterson, L. Melecio-Zambrano, C. Q. Trainor, B. P. Fors and H. D. Abruña, *J. Mater. Chem. A*, 2021, **9**, 5657–5663.

164 L. Huang, Y. Chen, Y. Liu, T. Wu, H. Li, J. Ye, G. Dai, X. Zhang and Y. Zhao, *ACS Sustainable Chem. Eng.*, 2020, **8**, 17868–17875.

165 S. Muench, A. Wild, C. Friebe, B. Häupler, T. Janoschka and U. S. Schubert, *Chem. Rev.*, 2016, **116**, 9438–9484.

166 T. Janoschka, M. D. Hager and U. S. Schubert, *Adv. Mater.*, 2012, **24**, 6397–6409.

167 J. Xie, P. Gu and Q. Zhang, *ACS Energy Lett.*, 2017, **2**, 1985–1996.

168 L. J. Fetters, D. J. Lohse, D. Richter, T. A. Witten and A. Zirkel, *Macromolecules*, 1994, **27**, 4639–4647.

169 D. Golodnitsky, E. Strauss, E. Peled and S. Greenbaum, *J. Electrochem. Soc.*, 2015, **162**, A2551.

170 E. B. Trigg, T. W. Gaines, M. Maréchal, D. E. Moed, P. Rannou, K. B. Wagener, M. J. Stevens and K. I. Winey, *Nat. Mater.*, 2018, **17**, 725–731.

171 M. Kolek, F. Otteny, P. Schmidt, C. Mück-Lichtenfeld, C. Einholz, J. Becking, E. Schleicher, M. Winter, P. Bieker and B. Esser, *Energy Environ. Sci.*, 2017, **10**, 2334–2341.

172 F. Otteny, V. Perner, D. Wassy, M. Kolek, P. Bieker, M. Winter and B. Esser, *ACS Sustainable Chem. Eng.*, 2020, **8**, 238–247.

173 H. Kye, Y. Kang, D. Jang, J. E. Kwon and B.-G. Kim, *Adv. Energy Sustainability Res.*, 2022, **3**, 2200030.

174 M. Kolek, F. Otteny, J. Becking, M. Winter, B. Esser and P. Bieker, *Chem. Mater.*, 2018, **30**, 6307–6317.

175 G. Dai, Y. Liu, Z. Niu, P. He, Y. Zhao, X. Zhang and H. Zhou, *Matter*, 2019, **1**, 945–958.

176 C. N. Gannett, B. M. Peterson, L. Shen, J. Seok, B. P. Fors and H. D. Abruña, *ChemSusChem*, 2020, **13**, 2428–2435.

177 Y. Wang, Y. Huang, Y. Hua, Y. Du and H. Yang, *New J. Chem.*, 2022, **46**, 14314–14317.

178 S. Xu, H. Dai, S. Zhu, Y. Wu, M. Sun, Y. Chen, K. Fan, C. Zhang, C. Wang and W. Hu, *eScience*, 2021, **1**, 60–68.

179 F. A. Obrezkov, A. I. Somova, E. S. Fedina, S. G. Vasil'ev, K. J. Stevenson and P. A. Troshin, *Energy Technol.*, 2021, **9**, 2000772.

180 X. Zhao, X. Qiu, H. Xue, S. Liu, D. Liang, C. Yan, W. Chen, Y. Wang and G. Zhou, *Angew. Chem.*, 2023, **135**, e202216713.

181 Q. He, S. Lv, Y. Huang, J. Guo, X. Peng, Y. Du and H. Yang, *RSC Adv.*, 2023, **13**, 12464–12468.

182 R. R. Kapaev, I. S. Zhidkov, E. Z. Kurmaev, K. J. Stevenson and P. A. Troshin, *J. Mater. Chem. A*, 2019, **7**, 22596–22603.

183 J. Wang, J. C. Z. En, S. N. Riduan and Y. Zhang, *Chem.–Eur. J.*, 2020, **26**, 2581–2585.

184 S. Lee, J. Hong, S.-K. Jung, K. Ku, G. Kwon, W. M. Seong, H. Kim, G. Yoon, I. Kang, K. Hong, H. W. Jang and K. Kang, *Energy Storage Mater.*, 2019, **20**, 462–469.

185 A. Wild, M. Strumpf, B. Häupler, M. D. Hager and U. S. Schubert, *Adv. Energy Mater.*, 2017, **7**, 1601415.

186 M. Lee, J. Hong, D.-H. Seo, D. H. Nam, K. T. Nam, K. Kang and C. B. Park, *Angew. Chem., Int. Ed.*, 2013, **52**, 8322–8328.

187 H. Banda, D. Damien, K. Nagarajan, A. Raj, M. Hariharan and M. M. Shaijumon, *Adv. Energy Mater.*, 2017, **7**, 1701316.

188 Y. Ji, K. Yang, M. Liu, S. Chen, X. Liu, B. Yang, Z. Wang, W. Huang, Z. Song and S. Xue, *Adv. Funct. Mater.*, 2021, **31**, 2104830.

189 A. Yu, C. Li, X. Chen, C. Zhang, S. Mei and C. J. Yao, *ChemSusChem*, 2024, **17**, e202301809.

190 F. Wang, J. Wang, G. Li, Z. Guo, J. Chu, X. Ai and Z. Song, *Energy Storage Mater.*, 2022, **50**, 658–667.

191 Z. Wang, A. Duan, W. Jin, X. Huang and Y. Li, *J. Mater. Chem. A*, 2022, **10**, 10026–10032.

192 M. Stolar, C. Reus and T. Baumgartner, *Adv. Energy Mater.*, 2016, **6**, 1600944.

193 T. Xia, T. Zhu, Y. Miao and X. Zhao, *ACS Appl. Energy Mater.*, 2022, **5**, 6980–6985.

194 T. Ma, L. Liu, J. Wang, Y. Lu and J. Chen, *Angew. Chem., Int. Ed.*, 2020, **59**, 11533–11539.

195 W. Sun, C. Zhou, Y. Fan, Y. He, H. Zhang, Z. Quan, H. Kong, F. Fu, J. Qin and Y. Shen, *Angew. Chem.*, 2023, **135**, e202300158.

196 T. Škorjanc, D. Shetty, M. A. Olson and A. Trabolsi, *ACS Appl. Mater. Interfaces*, 2019, **11**, 6705–6716.

197 K. Madasamy, D. Velayutham, V. Suryanarayanan, M. Kathiresan and K.-C. Ho, *J. Mater. Chem. C*, 2019, **7**, 4622–4637.

198 M. Kathiresan, B. Ambrose, N. Angulakshmi, D. E. Mathew, D. Sujatha and A. M. Stephan, *J. Mater. Chem. A*, 2021, **9**, 27215–27233.

199 S. M. Beladi-Mousavi, S. Sadaf, A. M. Mahmood and L. Walder, *ACS Nano*, 2017, **11**, 8730–8740.

200 V. Kolivoška, M. Gál, L. Pospíšil, M. Valášek and M. Hromadová, *Phys. Chem. Chem. Phys.*, 2011, **13**, 11422–11429.

201 W. Haiss, H. van Zalinge, H. Höbenreich, D. Bethell, D. J. Schiffrin, S. J. Higgins and R. J. Nichols, *Langmuir*, 2004, **20**, 7694–7702.

202 M. J. Lacey, J. T. Frith and J. R. Owen, *Electrochem. Commun.*, 2013, **26**, 74–76.

203 M. Yao, H. Sano, H. Ando and T. Kiyobayashi, *Sci. Rep.*, 2015, **5**, 10962.

204 Z. Wang, A. Duan, W. Jin, X. Huang and Y. Li, *J. Mater. Chem. A*, 2022, **10**, 10026–10032.

205 H. Nishide and K. Oyaizu, *Science*, 2008, **319**, 737–738.

206 J. Qu, T. Katsumata, M. Satoh, J. Wada, J. Igarashi, K. Mizoguchi and T. Masuda, *Chem.–Eur. J.*, 2007, **13**, 7965–7973.

207 H. Nishide, S. Iwasa, Y.-J. Pu, T. Suga, K. Nakahara and M. Satoh, *Electrochim. Acta*, 2004, **50**, 827–831.

208 Y. Xie, K. Zhang, Y. Yamauchi, K. Oyaizu and Z. Jia, *Mater. Horiz.*, 2021, **8**, 803–829.

This journal is © The Royal Society of Chemistry 2025

J. Mater. Chem. A, 2025, **13**, 1552–1589 | **1587**

209 T. Suga, Y.-J. Pu, S. Kasatori and H. Nishide, *Macromolecules*, 2007, **40**, 3167–3173.

210 T. Suga, S. Sugita, H. Ohshiro, K. Oyaizu and H. Nishide, *Adv. Mater.*, 2011, **6**, 751–754.

211 J. C. Barbosa, A. Fidalgo-Marijuan, J. C. Dias, R. Gonçalves, M. Salado, C. M. Costa and S. Lanceros-Méndez, *Energy Storage Mater.*, 2023, **60**, 102841.

212 H. Nishide and T. Suga, *Electrochem. Soc. Interface*, 2005, **14**, 32.

213 M. Suguro, S. Iwasa, Y. Kusachi, Y. Morioka and K. Nakahara, *Macromol. Rapid Commun.*, 2007, **28**, 1929–1933.

214 K. Nakahara, J. Iriyama, S. Iwasa, M. Suguro, M. Satoh and E. J. Cairns, *J. Power Sources*, 2007, **165**, 398–402.

215 J.-K. Kim, Y. Kim, S. Park, H. Ko and Y. Kim, *Energy Environ. Sci.*, 2016, **9**, 1264–1269.

216 K. Koshika, N. Sano, K. Oyaizu and H. Nishide, *Macromol. Chem. Phys.*, 2009, **210**, 1989–1995.

217 W. Deng, W. Shi, Q. Liu, J. Jiang, Q. Wang and C. Guo, *J. Power Sources*, 2020, **479**, 228796.

218 W. Jin, T. Zhou, Z. Wang, W. Xue, C. Feng, F. Zhang, X. Huang, D. Yang, P. Théato and Y. Li, *J. Power Sources*, 2021, **511**, 230363.

219 K. Zhang, Y. Hu, L. Wang, M. J. Monteiro and Z. Jia, *ACS Appl. Mater. Interfaces*, 2017, **9**, 34900–34908.

220 S. Yeşilot, F. Hacıvelioğlu, S. Küçükköylü, E. Demir, K. B. Celik and R. Demir-Cakan, *Polym. Adv. Technol.*, 2019, **30**, 2977–2982.

221 H. Byeon, B. Gu, H.-J. Kim, J. H. Lee, I. Seo, J. Kim, J. W. Yang and J.-K. Kim, *Chem. Eng. J.*, 2021, **413**, 127402.

222 T. Zhou, W. Jin, W. Xue, B. Dai, C. Feng, X. Huang, P. Théato and Y. Li, *J. Power Sources*, 2021, **483**, 229136.

223 K. Zhang, Y. Hu, L. Wang, J. Fan, M. J. Monteiro and Z. Jia, *Polym. Chem.*, 2017, **8**, 1815–1823.

224 J.-K. Kim, *J. Power Sources*, 2020, **477**, 228670.

225 Y. Chen, Y. Zhang, X. Liu, X. Fan, B. Bai, K. Yang, Z. Liang, Z. Zhang and K. Mai, *Macromol. Rapid Commun.*, 2018, **39**, 1800195.

226 A. Gopinath and A. S. Nasar, *Polymer*, 2019, **178**, 121601.

227 N. Hergué, B. Ernould, A. Minoia, R. Lazzaroni, J.-F. Gohy, P. Dubois and O. Coulembier, *Batteries Supercaps*, 2018, **1**, 102–109.

228 P. G. Bruce, S. A. Freunberger, L. J. Hardwick and J.-M. Tarascon, *Nat. Mater.*, 2012, **11**, 19–29.

229 B. Dunn, J.-M. Kamath and J. M. Tarascon, *Science*, 2011, **334**, 928–935.

230 V. Etacheri, R. Marom, R. Elazari, G. Salitra and D. Aurbach, *Energy Environ. Sci.*, 2011, **4**, 3243–3262.

231 C. Zhang, S. Chen, G. Zhou, Q. Hou, S. Luo, Y. Wang and G. Shi, *J. Electrochem. Soc.*, 2021, **168**, 050548.

232 Y. Zhao, M. Wu, H. Zhang, Z. Ge, C. Li, Y. Ma and Y. Chen, *Energy Storage Mater.*, 2022, **47**, 141–148.

233 W. Wang, C. Zhao, J. Yang, P. Xiong, H. Su and Y. Xu, *Sci. China Mater.*, 2021, **64**, 2938–2948.

234 B. Wei, Y. Hong, W. Tang, M. Guo, X. He, C. Tang, J. Hu and C. Fan, *Chem. Eng. J.*, 2023, **451**, 138773.

235 C.-X. Zhang, X.-H. Chen, W.-S. Zhang, Y. Wang, S.-L. Mei, Y.-W. Zhong and C.-J. Yao, *Chem. Eng. J.*, 2024, **483**, 149198.

236 T. Liu, K. C. Kim, B. Lee, S. Jin, M. J. Lee, M. Li, S. Noda, S. S. Jang and S. W. Lee, *ACS Appl. Energy Mater.*, 2020, **3**, 3728–3735.

237 H. Guo, L. Liu, H. Shu, X. Yang, Z. Yang, M. Zhou, J. Tan, Z. Yan, H. Hu and X. Wang, *J. Power Sources*, 2014, **247**, 117–126.

238 L. Zhu, L. Xie and X. Cao, *ACS Appl. Mater. Interfaces*, 2018, **10**, 10909–10917.

239 P.-O. Schwartz, S. Förtsch, E. Mena-Osteritz, D. Weirather-Köstner, M. Wachtler and P. Bäuerle, *RSC Adv.*, 2018, **8**, 14193–14200.

240 L. Zhu, L. Xie, C. Bao, X. Yan and X. Cao, *Int. J. Energy Res.*, 2020, **44**, 298–308.

241 X. Li, X. Tang, K. Ouyang, P. Deng, L. Huang and W. Dang, *Ionics*, 2021, **27**, 4649–4661.

242 F. Wu, J. Liu, L. Li, X. Zhang, R. Luo, Y. Ye and R. Chen, *ACS Appl. Mater. Interfaces*, 2016, **8**, 23095–23104.

243 J. Yang, Y. Shi, M. Li, P. Sun and Y. Xu, *ACS Appl. Mater. Interfaces*, 2020, **12**, 32666–32672.

244 G. Hernández, N. Casado, R. Coste, D. Shanmukaraj, L. Rubatat, M. Armand and D. Mecerreyes, *RSC Adv.*, 2015, **5**, 17096–17103.

245 L. Assumma, Y. Kervella, J. M. Mouesca, M. Mendez, V. Maurel, L. Dubois, T. Gutel and S. Sadki, *ChemSusChem*, 2020, **13**, 2419–2427.

246 C.-J. Yao, J. Xie, Z. Wu, Z. J. Xu, S. Zhang and Q. Zhang, *Chem.–Asian J.*, 2019, **14**, 2210–2214.

247 S. Zheng, L. Miao, T. Sun, L. Li, T. Ma, J. Bao, Z. Tao and J. Chen, *J. Mater. Chem. A*, 2021, **9**, 2700–2705.

248 H. Zhang, Y. Xie, X. Chen, T. Jia, W. Huang, S. Luo, Q. Hou, R. Zeng and Z. Sun, *J. Electrochem. Soc.*, 2017, **164**, A290.

249 S. Wang, A. M. G. Park, P. Flouda, A. D. Easley, F. Li, T. Ma, G. D. Fuchs and J. L. Lutkenhaus, *ChemSusChem*, 2020, **13**, 2371–2378.

250 P. Acker, J. S. Wössner, G. Desmaizieres and B. Esser, *ACS Sustainable Chem. Eng.*, 2022, **10**, 3236–3244.

251 Z. Chen, S. Mei, W. Li, N. Xu, Y. Dong, Y. Jin, M. Ouyang and C. Zhang, *J. Mater. Chem. A*, 2021, **9**, 27010–27018.

252 J. Wang, Y. Lee, K. Tee, S. N. Riduan and Y. Zhang, *Chem. Commun.*, 2018, **54**, 7681–7684.

253 R. Akiyoshi, M. Fujiwara, Y. Kamakura, T. Shimizu, R. Inoue, Y. Morisaki, A. Saeki, H. Yoshikawa and D. Tanaka, *ACS Appl. Energy Mater.*, 2022, **5**, 12760–12767.

254 N. Cheng, L. Ren, X. Xu, Y. Du and S. X. Dou, *Mater. Today Phys.*, 2020, **15**, 100289.

255 T. Mehtab, G. Yasin, M. Arif, M. Shakeel, R. M. Korai, M. Nadeem, N. Muhammad and X. Lu, *J. Energy Storage*, 2019, **21**, 632–646.

256 G. Zhang, C. Xie, P. You and S. Li, in *Introduction to Organic Electronic Devices*, ed. G. Zhang, C. Xie, P. You and S. Li, Springer Nature Singapore, Singapore, 2022, pp. 283–307.

257 L. Wang, Y. Han, X. Feng, J. Zhou, P. Qi and B. Wang, *Coord. Chem. Rev.*, 2016, **307**, 361–381.

258 G. Xu, P. Nie, H. Dou, B. Ding, L. Li and X. Zhang, *Mater. Today*, 2017, **20**, 191–209.

1588 | *J. Mater. Chem. A*, 2025, **13**, 1552–1589

This journal is © The Royal Society of Chemistry 2025

259 X. Chen, W. Sun and Y. Wang, *ChemElectroChem*, 2020, **7**, 3905–3926.

260 Y. Deng, Y. Wang, X. Xiao, B. J. Saucedo, Z. Zhu, M. Xie, X. Xu, K. Yao, Y. Zhai and Z. Zhang, *Small*, 2022, **18**, 2202928.

261 H. Kong, Y. Guan, J. Wang, W. Sun, L. Chen, J. Ou, L. Xie, F. Fu, H. Zhang and H. Chen, *J. Mater. Chem. A*, 2022, **10**, 20866–20873.

262 X. Du, Z. Zhang, W. Liu and Y. Deng, *Nano Energy*, 2017, **35**, 299–320.

263 X. Yao and Y. Zhao, *Chem*, 2017, **2**, 171–200.

264 P. Sengodu and A. D. Deshmukh, *RSC Adv.*, 2015, **5**, 42109–42130.

265 S. Maiti, A. Pramanik, T. Dhawa and S. Mahanty, *Mater. Lett.*, 2017, **209**, 613–617.

266 H.-C. Lin, C.-C. Li and J.-T. Lee, *J. Power Sources*, 2011, **196**, 8098–8103.

267 J.-Y. Shi, C.-W. Yi and K. Kim, *Bull. Korean Chem. Soc.*, 2010, **31**, 2698–2700.

268 W.-M. Chen, L. Qie, L.-X. Yuan, S.-A. Xia, X.-L. Hu, W.-X. Zhang and Y.-H. Huang, *Electrochim. Acta*, 2011, **56**, 2689–2695.

269 Z. Peng, X. Yi, Z. Liu, J. Shang and D. Wang, *ACS Appl. Mater. Interfaces*, 2016, **8**, 14578–14585.

270 J. Wang, W. Zhang, H. Wei, X. Zhai, F. Wang, Y. Zhou, F. Tao, P. Zhai, W. Liu and Y. Liu, *Sustainable Energy Fuels*, 2022, **6**, 2901–2923.

271 S. Lei, Y. Dong, Y. Dou, X. Zhang, Q. Zhang and Y. Yang, *Mater. Adv.*, 2021, **2**, 5785–5790.

272 P. Das and B. C. Thompson, *Polym. J.*, 2023, **55**, 317–341.

273 K.-L. Wang, K.-T. Chen, Y.-H. Yi, Y.-H. Hung, H.-Y. Tuan and M. Horie, *ACS Sustainable Chem. Eng.*, 2020, **8**, 1043–1049.

274 V. V. Kondratiev and R. Holze, *Chem. Pap.*, 2021, **75**, 4981–5007.

275 C. Liedel, X. Wang and M. Antonietti, *Nano Energy*, 2018, **53**, 536–543.

276 P. Acker, L. Rzesny, C. F. N. Marchiori, C. M. Araujo and B. Esser, *Adv. Funct. Mater.*, 2019, **29**, 1906436.

This journal is © The Royal Society of Chemistry 2025

J. Mater. Chem. A, 2025, **13**, 1552–1589 | **1589**